

Characteristics of profiles of gamma-ray burst pulses associated with the Doppler effect of fireballs

Yi-Ping Qin^{1,2,4}, Zhi-Bin Zhang^{1,3}, Fu-Wen Zhang² and Xiao-Hong Cui^{1,3}

¹National Astronomical Observatories/Yunnan Observatory, Chinese Academy of Sciences, P. O. Box 110, Kunming, Yunnan, 650011, P. R. China

²Physics Department, Guangxi University, Nanning, Guangxi, 530004, P. R. China

³ The Graduate School of the Chinese Academy of Sciences

⁴ E-mail:ypqin@public.km.yn.cn

Abstract

In this paper, we derive in a much detail the formula of count rates, in terms of the integral of time, of gamma-ray bursts in the framework of fireballs, where the Doppler effect of the expanding fireball surface is the key factor to be concerned. Effects arising from the limit of the time delay due to the limited regions of the emitting areas in the fireball surface and other factors are investigated. Our analysis shows that the formula of the count rate of fireballs can be expressed as a function of τ which is the observation time scale relative to the dynamical time scale of the fireball defined by R_c/c where R_c is the fireball radius measured at an associated local time. The profile of light curves of fireballs depends only on the relative time scale, entirely independent of the real time scale and the real size of the objects. It displays in detail how a cutoff tail, or a turn over, feature (called a cutoff tail problem) in the decay phase of a light curve can be formed. This feature is a consequence of a hot spot in the fireball surface, moving towards the observer, and was observed in a few cases previously. Local pulses suddenly dimming would produce light curves bearing a certain decaying form (called a standard decaying form) and exhibiting a sharp feature at their peaks. Light curves arising from gradually dimming local pulses would be smooth at their peaks, and their profiles in the decaying phase would obviously deviate from the standard form when the width of the local pulse is large enough. It is observed that light curves arising from relatively short local pulses would be the same, entirely independent of the shape of the latter. Impacts of the rest frame radiation form and the variance of the form on the profile of light curves are insignificant,

while that on the magnitude of the light curves would be obvious. By performing fits to the count rate light curves of six sample sources, we show how to obtain some physical parameters from the observed profile of the count rate of GRBs and show that there do exist some GRBs that the profiles of their count rate light curves can be described by the formula provided. In addition, the analysis reveals that the Doppler effect of fireballs could lead to a power law relationship between the *FWHM* of pulses and energy, which were observed previously by many authors.

Key words: gamma-rays: bursts — gamma-rays: theory — relativity

1 Introduction

Light curves of gamma-ray bursts (GRBs) vary enormously, suggesting that the temporal activity of the sources would be of a stochastic process (see, e.g., Fishman et al. 1994). However, some simple bursts with well-separated structure suggest that they may consist of fundamental units of emission such as pulses, and some pulses are seen to comprise a fast rise and an exponential decay (FRED), which can be well represented by an flexible empirical function (see, e.g., Norris et al. 1996).

Due to the observed great output rate of radiation, GRBs are assumed to undergo a stage of fireballs which expand relativistically (see, e.g., Goodman 1986; Paczynski 1986). As pointed out by Krolik & Pier (1991), relativistic bulk motion of the gamma-ray-emitting plasma can account for some phenomena of GRBs. For example, emission lines would be significantly broadened due to the curvature of the fireball surface where Doppler boosting factors varies from point to point (see, e.g., Mészáros & Rees 1998; Heiley et al. 1999; Qin 2003). Promisingly, the observed FRED structure was found to be interpreted by the curvature effect as the observed plasma moves relativistically towards us and appears to be locally isotropic (e.g., Fenimore et al. 1996, hereafter Paper I; Ryde & Petrosian 2002, hereafter Paper II; Kocevski et al. 2003). Taking into account the delay of the observational time from the area concerned, estimated by assuming $\theta \sim 1/\Gamma$, where θ is the angle to the line of sight and Γ is the Lorentz factor of the expansion, light curves affected by the curvature effect are available. As derived in detail in Paper II, a FRED pulse can be well described by the bolometric light curve of a shell shining continuously, which is

$$F(t) = F_0 \int_0^\infty \frac{f(t-x)}{(1+x/t_{ang})^2} dx, \quad (1)$$

where t_{ang} is the curvature timescale.

The motivations of the study of this paper are as follows. First, we want to know how the light curve looks like if only the emission of a hot spot is concerned, since there could be some on the fireball surface, probably of the size of $1/\Gamma$, and how the viewing angle of the spot plays a role. Second, we think it deserved to be investigated that if and how a rest frame radiation form plays a role on producing the light curve. Third, it would be interesting to know if and how other factors such as the width and the structure of local pulses affect the profile of the light curve observed, which also deserves a detail investigation.

In the following, we will first derive in a much detail the formula suitable for describing the light curve of fireballs expanding with any velocities so that it would be applicable to relativistic, sub-relativistic, or even non-relativistic motions (where, we will pay much of our attention to the integral limit which might be constrained by the concerned area of the fireball surface and/or the emission interval of time). Then we will apply the formula to the case of a local δ function pulse and show in detail how the light curve produced by a fraction of the fireball surface confined by $\theta \leq 1/\Gamma$ differs from that of the whole fireball surface, and how the light curve would be affected if the patch moving in a direction other than the line of sight. Later we will study light curves of different forms and different widths of local pulses. Impacts of the rest frame radiation form on the profile of light curves will also be investigated. Applications and discussion will be presented in late sections.

2 General formula of count rates for expanding fireballs

There are several papers published studying light curves of relativistically expanding fireballs (e.g., Paper I; Paper II). We present in the following a much detailed study on the same issue, where, we do not limit the expanding speed so that the result would be applicable to relativistic, sub-relativistic, or even non-relativistic motions, and much of our attention will be paid to the integral limit which might be constrained by the concerned area of the fireball surface as well as the emission interval of time. In this paper we consider the case of a fireball expanding isotropically with a constant Lorentz factor $\Gamma > 1$.

For a radiation independent of direction, the expected flux of a fireball expanding with a

constant Lorentz factor is (Qin 2002, hereafter Paper III)

$$f_\nu(t) = \frac{2\pi}{D^2} \int_{\tilde{\theta}_{\min}}^{\tilde{\theta}_{\max}} I_\nu(t_\theta, \nu) R^2(t_\theta) \cos \theta \sin \theta d\theta, \quad (2)$$

where ν is the observation frequency; t is the observation time; D is the distance of the fireball to the observer; θ is the angle, of the concerned differential surface ds_θ , of the fireball, to the line of sight; t_θ is the emission time (in the observer frame), called local time, of photons which emit from ds_θ ; $I_\nu(t_\theta, \nu)$ is the observer frame intensity; $R(t_\theta)$ is the radius of the fireball at time t_θ . The integral range of θ , $\tilde{\theta}_{\min}$ and $\tilde{\theta}_{\max}$, will be determined by the concerned area of the fireball surface as well as the emission ranges of the frequency and the local time. Applying the relation between the radius of the fireball and the observation time (see Paper III) we come to the following form of the flux:

$$f_\nu(t) = \frac{2\pi c^2 [(t - t_c - \frac{D}{c})\beta + \frac{R_c}{c}]^2}{D^2} \int_{\tilde{\theta}_{\min}}^{\tilde{\theta}_{\max}} \frac{I_\nu(t_\theta, \nu) \cos \theta \sin \theta}{(1 - \beta \cos \theta)^2} d\theta, \quad (3)$$

where t_c and R_c are constants.

Assume that the area of the fireball surface concerned is confined within

$$\theta_{\min} \leq \theta \leq \theta_{\max} \quad (4)$$

and the emission time t_θ is confined within

$$t_c \leq t_{\theta, \min} \leq t_\theta \leq t_{\theta, \max}, \quad (5)$$

and besides them there are no other constraints to the integral limit of (2) or (3). According to (4) and (5), one can verify that the lower and upper integral limits of (3) could be determined by

$$\tilde{\theta}_{\min} = \cos^{-1} \min \left\{ \cos \theta_{\min}, \frac{t_{\theta, \max} - t + \frac{D}{c}}{(t_{\theta, \max} - t_c)\beta + \frac{R_c}{c}} \right\} \quad (6)$$

and

$$\tilde{\theta}_{\max} = \cos^{-1} \max \left\{ \cos \theta_{\max}, \frac{t_{\theta, \min} - t + \frac{D}{c}}{(t_{\theta, \min} - t_c)\beta + \frac{R_c}{c}} \right\}, \quad (7)$$

respectively (for a detailed derivation, one could refer to Paper III).

As shown by Paper III, t_θ and t are related by

$$t_\theta = \frac{t - t_c - \frac{D}{c} + \frac{R_c}{c} \cos \theta}{1 - \beta \cos \theta} + t_c. \quad (8)$$

From (8) one finds that, for any given values of t and θ , t_θ would be uniquely determined. If this value of t_θ is within the range of (5), then there will be photons emitted at t_θ from the small

surface area of θ reaching the observer at t [when θ is within the range of (4), this small area would be included in the above integral, otherwise it would not]. Obviously, for a certain value of θ , the range of t depends on the range of t_θ . Inserting (8) into (5) and applying (4) we obtain

$$\begin{aligned} (1 - \beta \cos \theta_{\min})t_{\theta,\min} + (t_c\beta - \frac{R_c}{c}) \cos \theta_{\min} + \frac{D}{c} &\leq t \\ &\leq (1 - \beta \cos \theta_{\max})t_{\theta,\max} + (t_c\beta - \frac{R_c}{c}) \cos \theta_{\max} + \frac{D}{c} . \end{aligned} \quad (9)$$

It suggests clearly that observation time t is limited when emission time t_θ is limited.

If during some period the radiation of the fireball is dominated by a certain mechanism, then within this interval of time the intensity can be expressed as:

$$I_\nu(t_\theta, \nu) = I(t_\theta)g_\nu(\nu) = I(t_\theta)\frac{g_{0,\nu}(\nu_{0,\theta})}{(1 - \beta \cos \theta)^3 \Gamma^3}, \quad (10)$$

where $\nu_{0,\theta}$ is the rest frame emission frequency corresponding to ν (they are related by the Doppler effect), $I(t_\theta)$ represents the development of the intensity magnitude in the observer frame, and $g_\nu(\nu)$ and $g_{0,\nu}(\nu_{0,\theta})$ describe the observer frame and the rest frame radiation mechanisms, respectively. In deriving the last equivalency, the Lorentz invariance of $g_\nu(\nu)/\nu^3$ and the Doppler effect are applied. Flux (3) then can be written as

$$f_\nu(t) = \frac{2\pi c^2 [(t - t_c - \frac{D}{c})\beta + \frac{R_c}{c}]^2}{D^2 \Gamma^3} \int_{\tilde{\theta}_{\min}}^{\tilde{\theta}_{\max}} \frac{I(t_\theta)g_{0,\nu}(\nu_{0,\theta}) \cos \theta \sin \theta}{(1 - \beta \cos \theta)^5} d\theta, \quad (11)$$

where $\tilde{\theta}_{\min}$ and $\tilde{\theta}_{\max}$ are determined by (6) and (7), respectively, $\nu_{0,\theta}$ and ν are related by the Doppler effect, and t is confined by (9).

Light curves of gamma-ray bursts are always presented in terms of count rates within an energy range. The count rate within energy channel $[\nu_1, \nu_2]$ is determined by

$$\frac{dn(t)}{dt} = \int_{\nu_1}^{\nu_2} \frac{f_\nu(t)}{h\nu} d\nu. \quad (12)$$

Applying (11) leads to

$$\frac{dn(t)}{dt} = \frac{2\pi c^2 [(t - t_c - \frac{D}{c})\beta + \frac{R_c}{c}]^2 \int_{\tilde{\theta}_{\min}}^{\tilde{\theta}_{\max}} \frac{I(t_\theta) \cos \theta \sin \theta}{(1 - \beta \cos \theta)^5} d\theta \int_{\nu_1}^{\nu_2} \frac{g_{0,\nu}(\nu_{0,\theta})}{\nu} d\nu}{hD^2 \Gamma^3}. \quad (13)$$

Assign

$$\tau_\theta \equiv \frac{t_\theta - t_c}{\frac{R_c}{c}}, \quad (14)$$

$$\tau_{\theta,\min} \equiv \frac{t_{\theta,\min} - t_c}{\frac{R_c}{c}}, \quad (15)$$

$$\tau_{\theta,\max} \equiv \frac{t_{\theta,\max} - t_c}{\frac{R_c}{c}}, \quad (16)$$

and

$$\tau \equiv \frac{t - t_c - \frac{D}{c} + \frac{R_c}{c}}{\frac{R_c}{c}}. \quad (17)$$

One would find

$$\tau_\theta = \frac{\tau - (1 - \cos \theta)}{1 - \beta \cos \theta}, \quad (18)$$

$$\tau_{\theta, \min} \leq \tau \leq \tau_{\theta, \max}, \quad (19)$$

and

$$1 - \cos \theta_{\min} + (1 - \beta \cos \theta_{\min})\tau_{\theta, \min} \leq \tau \leq 1 - \cos \theta_{\max} + (1 - \beta \cos \theta_{\max})\tau_{\theta, \max} \quad (20)$$

[which is the range of τ within which the radiation defined within (4) and (5) is observable].

One could verify that, in terms of the integral of τ_θ , count rate (13) becomes

$$C(\tau) = \frac{2\pi R_c^3 \int_{\tilde{\tau}_{\theta, \min}}^{\tilde{\tau}_{\theta, \max}} \tilde{I}(\tau_\theta) (1 + \beta \tau_\theta)^2 (1 - \tau + \tau_\theta) d\tau_\theta \int_{\nu_1}^{\nu_2} \frac{g_{0,\nu}(\nu_{0,\theta})}{\nu} d\nu}{hcD^2 \Gamma^3 (1 - \beta)^2 (1 + k\tau)^2}, \quad (21)$$

where τ is confined by (20),

$$C(\tau) \equiv \frac{dn[t(\tau)]}{d\tau}, \quad (22)$$

$$\tilde{I}(\tau_\theta) \equiv I[t_\theta(\tau_\theta)], \quad (23)$$

$$k \equiv \frac{\beta}{1 - \beta}, \quad (24)$$

and $\nu_{0,\theta}$ and ν are related by

$$\nu_{0,\theta} = \frac{(1 + k\tau)(1 - \beta)\Gamma}{1 + \beta\tau_\theta} \nu, \quad (25)$$

while $\tilde{\tau}_{\theta, \min}$ and $\tilde{\tau}_{\theta, \max}$ are determined by

$$\tilde{\tau}_{\theta, \min} = \max\left\{\tau_{\theta, \min}, \frac{\tau - 1 + \cos \theta_{\max}}{1 - \beta \cos \theta_{\max}}\right\} \quad (26)$$

and

$$\tilde{\tau}_{\theta, \max} = \min\left\{\tau_{\theta, \max}, \frac{\tau - 1 + \cos \theta_{\min}}{1 - \beta \cos \theta_{\min}}\right\}, \quad (27)$$

respectively.

Taking $t_\theta = t_c$, we then find from (8) that photons emitted from $\theta = 0$ and at local time t_c would reach the observer at observation time $t = t_c + D/c - R_c/c$. Thus, the term of $t - t_c - D/c + R_c/c$ in (17) represents the interval between the observation time of a photon and that of the photons emitted from $\theta = 0$ and at local time t_c . Therefore, as (17) suggests, τ indicates the above time interval relative to the dynamical time scale of the fireball defined by R_c/c where R_c is the fireball

radius measured at local time t_c (note that t_c is a local time based on it τ is defined). Formula (21) shows that the profile of count rates of a fireball source is a function of τ . It is independent of the real time scale $t - t_c - D/c + R_c/c$, and independent of the real size, R_c , of the source. In other words, no matter how large is the fireball concerned and how large is the observed timescale concerned, for the profile of the count rate, only the ratio of the latter to the dynamical time scale of the fireball plays a role.

3 Count rate of local δ function pulses

Previous studies on the light curve of a local δ function pulse can be found in Papers I and II, where, as mentioned above, the limit of the time delay due to the constraint of the finite emission region is ignored. Here, we study the same light curve by applying the formula of count rates derived above, in which, the mentioned constraint is taken into account and, in addition, other factors possibly ignored by previous studies will be presented.

Let

$$I(t_\theta) = I_0 \delta(t_\theta - t_{\theta,0}) \quad (t_{\theta,\min} \leq t_\theta \leq t_{\theta,\max}), \quad (28)$$

with

$$t_{\theta,\min} < t_{\theta,0} < t_{\theta,\max}, \quad (29)$$

where I_0 is a constant. In terms of τ_θ , we would get

$$\tilde{I}(\tau_\theta) = \frac{cI_0}{R_c} \delta(\tau_\theta - \tau_{\theta,0}) \quad (\tau_{\theta,\min} \leq \tau_\theta \leq \tau_{\theta,\max}) \quad (30)$$

and

$$\tau_{\theta,\min} < \tau_{\theta,0} < \tau_{\theta,\max}, \quad (31)$$

where

$$\tau_{\theta,0} \equiv \frac{t_{\theta,0} - t_c}{\frac{R_c}{c}}. \quad (32)$$

One can check that, when

$$1 - \cos \theta_{\min} + (1 - \beta \cos \theta_{\min})\tau_{\theta,0} < \tau < 1 - \cos \theta_{\max} + (1 - \beta \cos \theta_{\max})\tau_{\theta,0} \quad (33)$$

(which is the range of τ within which the radiation of the local δ function pulse over the concerned area is observable), the following would be satisfied:

$$\tilde{\tau}_{\theta,\min} < \tau_{\theta,0} < \tilde{\tau}_{\theta,\max}. \quad (34)$$

Inserting (30) into (21) and applying (34) one would get

$$C(\tau) = \frac{2\pi R_c^2 I_0 \int_{\nu_1}^{\nu_2} \frac{g_{0,\nu}(\nu_{0,\theta})}{\nu} d\nu}{hD^2} C_0(\tau), \quad (35)$$

where τ is confined by (33),

$$C_0(\tau) \equiv \frac{(1 + \beta\tau_{\theta,0})^2(1 + \tau_{\theta,0} - \tau)}{\Gamma^3(1 - \beta)^2(1 + k\tau)^2} \quad (36)$$

and

$$\nu_{0,\theta} = \frac{(1 + k\tau)(1 - \beta)\Gamma}{1 + \beta\tau_{\theta,0}} \nu. \quad (37)$$

It shows that, due to the Doppler effect (or the curvature effect) referring to the concerned area in the fireball surface, a local δ function pulse would produce an observed pulse bearing the shape of $C_0(\tau)$, where τ is confined by (33), modified by the rest frame spectrum of the fireball.

First, let us consider the radiation emitted from the whole fireball surface (called emitting area 1). In this case we take

$$\theta_{\min} = 0 \quad \text{and} \quad \theta_{\max} = \frac{\pi}{2}, \quad (38)$$

and get from (33) that

$$(1 - \beta)\tau_{\theta,0} < \tau < 1 + \tau_{\theta,0}. \quad (39)$$

Adopting $\tau_{\theta,0} = 0$, we get $0 < \tau < 1$. Presented in Fig. 1 are the curves of $C_0(\tau)$ corresponding to $\Gamma = 10$ and $\Gamma = 100$, respectively. The figure shows that, function $C_0(\tau)$ confined by (39) bears a feature of an exponential decay, and the profile remains the same for different values of the Lorentz factor. It is interesting that the upper limit of τ [see (39)] does not prevent the formation of the exponential decay tail.

One can verify that, the maximum value of $C_0(\tau)$ is

$$C_{0,p} = \frac{1}{\Gamma(\Gamma - \sqrt{\Gamma^2 - 1})^2} \frac{R(t_{\theta,0})}{R_c}, \quad (40)$$

while the width of $C_0(\tau)$ can be determined by

$$\Delta\tau_{FWHM} = \frac{(\Gamma - \sqrt{\Gamma^2 - 1})(\sqrt{2\Gamma^2 - 1} - \Gamma)}{\Gamma^2 - 1} \frac{R(t_{\theta,0})}{R_c}, \quad (41)$$

and the relation between them is

$$C_{0,p} = \frac{\Gamma^2 - 1}{\Gamma(\Gamma - \sqrt{\Gamma^2 - 1})^3(\sqrt{2\Gamma^2 - 1} - \Gamma)} \Delta\tau_{FWHM}. \quad (42)$$

(For a detailed derivation one could refer to Appendix A).

Ignoring the effect of the rest frame radiation form (which will be discussed below), $C_{0,p}$ and $\Delta\tau_{FWHM}$ will serve as the observed peak and width of the light curve of the local δ function pulse. When $\Gamma \gg 1$, one can come to

$$C_{0,p} \simeq 4\Gamma \frac{R(t_{\theta,0})}{R_c} \quad (\Gamma \gg 1), \quad (43)$$

$$\Delta\tau_{FWHM} \simeq \frac{\sqrt{2}-1}{2\Gamma^2} \frac{R(t_{\theta,0})}{R_c} \quad (\Gamma \gg 1), \quad (44)$$

and

$$C_{0,p} \simeq \frac{8\Gamma^3}{\sqrt{2}-1} \Delta\tau_{FWHM} \quad (\Gamma \gg 1). \quad (45)$$

It shows, both the observed peak and width of the count rate of the local δ function pulse are proportional to the size of the fireball. While the former rises linearly with the increase of the Lorentz factor, the latter, as generally known, decays rapidly following the law of Γ^{-2} (see, e.g. Fenimore et al. 1993), which naturally explains why for many bursts very short time scales, as small as a few *ms*, of pulses have been observed. For a certain value of the Lorentz factor, quantities $C_{0,p}$ and $\Delta\tau_{FWHM}$ are proportional to each other.

Combining (43) and (44) one gets

$$C_{0,p}^2 \Delta\tau_{FWHM} \simeq 8(\sqrt{2}-1) \left(\frac{R(t_{\theta,0})}{R_c}\right)^3 \quad (\Gamma \gg 1). \quad (46)$$

This suggests that, for a same kind of fireball sources, if their difference is merely due to the Lorentz factor, the product of the square of the peak count rate and the width of the light curve of their very narrow local pulses would be the same. This provides a statistical approach to test the fireball model with pulses of GRBs. For a source, if the intensity of its pulses remains unchanged, one can expect a high pulse coupling with a small width while a low pulse coupling with a larger one.

Let $\Delta\tau$ be the interval of the observable time of the local δ function pulse. It would be determined by (39). According to (A6) and (A8) we get

$$\frac{R(t_{\theta,0})}{R_c} = \Delta\tau. \quad (47)$$

Then (44) becomes

$$\Delta\tau_{FWHM} \simeq \frac{\sqrt{2}-1}{2\Gamma^2} \Delta\tau \quad (\Gamma \gg 1). \quad (48)$$

With this one finds that the observed width of the light curve of the local δ function pulse would be several orders of magnitude smaller than the limit of the observable time when the Lorentz

factor is large enough. This explains why the upper limit of τ does not prevent the formation of the exponential decay tail shown in Fig. 1.

Let us turn to study the effect of the limit of the time delay, which refers to the radiation emitted from a small area with $\theta \leq 1/\Gamma$ (called emitting area 2). Taking

$$\theta_{\min} = 0 \quad \text{and} \quad \theta_{\max} = \frac{1}{\Gamma}, \quad (49)$$

we get from (33) that

$$(1 - \beta)\tau_{\theta,0} < \tau < 1 - \cos \frac{1}{\Gamma} + (1 - \beta \cos \frac{1}{\Gamma})\tau_{\theta,0}, \quad (50)$$

when Γ is large enough which would lead to

$$(1 - \beta)\tau_{\theta,0} < \tau < \frac{1 + 2\tau_{\theta,0}}{2\Gamma^2} \quad (\Gamma \gg 1). \quad (51)$$

Adopting $\tau_{\theta,0} = 0$, we get $0 < \tau < 1/2\Gamma^2$. The curves of $C_0(\tau) - \tau$ for $\Gamma = 10$ and 100 in this case are also presented in Fig. 1. It shows that, due to the curvature effect, neglecting the area of $\theta > 1/\Gamma$ would lead a light curve, of a local δ function pulse, with a cutoff tail in its decay phase, which we call a cutoff tail problem, suggesting that if only the radiation emitted from the area of $\theta < 1/\Gamma$ is considered, the decay phase of the corresponding light curve would not be a full exponentially decaying one (the case of a longer local pulse will be discussed in late sections). [A similar result can be deduced from the dot lines presented in Fig. 4 of Paper I.] As shown in Appendix A, the count rate at $\theta = 1/\Gamma$ is a quarter of the peak, and hence the missed part of the light curve is obviously observable.

What considered above is a patch, with the area of $\theta \leq 1/\Gamma$, moving towards the observer. What would one expect if the patch moving in a direction other than the line of sight? Light curves arising from a small area in the fireball surface, confined by $\theta - \theta + d\theta$ and $\varphi - \varphi + d\varphi$, can be calculated by taking $\theta_{\min} = \theta$ and $\theta_{\max} = \theta + d\theta$ and then multiplying the resulted $C_0(\tau)$ and $d\varphi/2\pi$. The second step works due to the highly symmetric nature of the surface. Any forms of patches can be divided into many small areas confined by $\theta_i - \theta_i + d\theta$ and $\varphi_i - \varphi_i + d\varphi$ and the light curves arising from these patches would be obtained by making a sum of the count rates of the corresponding small areas. Here we consider a simple case, the radiation emitted from a patch which is confined by

$$\theta_{\min} = \frac{1}{2\Gamma}, \quad \theta_{\max} = \frac{3}{2\Gamma}; \quad \Delta\varphi = \pi, \quad (52)$$

(called emitting area 3). The viewing angle of the center of this patch is $\sim 1/\Gamma$ and its size is almost the same as the previous one. We get from (33) that

$$1 - \cos \frac{1}{2\Gamma} + (1 - \beta \cos \frac{1}{2\Gamma})\tau_{\theta,0} < \tau < 1 - \cos \frac{3}{2\Gamma} + (1 - \beta \cos \frac{3}{2\Gamma})\tau_{\theta,0}. \quad (53)$$

Once more, we adopt $\tau_{\theta,0} = 0$. The curves of $C_0(\tau) - \tau$ for $\Gamma = 10$ and 100 in this case are presented in Fig. 1 as well. Shown in this figure, the feature of cutoff tails is also observed. Compared with that of the previous patch (emitting area 2), the light curves last a much longer time, while the amplitudes are much smaller.

Comparing the light curves associated with $\Gamma = 10$ and 100 we find that, the profiles of the curves corresponding to different Lorentz factors are not distinguishable, as long as Γ is large enough to represent a relativistic motion.

Compared with that presented in Papers I and II, one finds from (36) that the factor of $(1 + \tau_{\theta,0} - \tau)$ was previously ignored. When $\tau \ll 1 + \tau_{\theta,0}$, this factor is negligible, while when τ is comparable to $1 + \tau_{\theta,0}$, this factor would play a role. However, as shown in Fig. 1, a large value of the Lorentz factor will make the decay phase of the light curve very short, so that the interesting value of τ will be very small and then the factor of $(1 + \tau_{\theta,0} - \tau)$ would not be important.

Another factor affecting the light curve is the integral of the rest frame radiation. When adopting $g_{0,\nu}(\nu_{0,\theta}) = \nu_{0,\theta}^{-\alpha_f}$, one obtains $\int_{\nu_1}^{\nu_2} [g_{0,\nu}(\nu_{0,\theta})/\nu] d\nu = g_0(1+k\tau)^{-\alpha_f}$, where g_0 is a constant. A product of this term with the term of $(1+k\tau)^{-2}$ in $C_0(\tau)$ is similar to that obtained in Paper I. However, observation suggests that the common radiation form of GRBs is the so-called Band function (Band et al. 1993) which was frequently, and rather successfully, employed to fit the spectra of the sources (see, e.g., Schaefer et al. 1994; Ford et al. 1995; Preece et al. 1998, 2000). Paper III shows that the observed radiation form would only be affected slightly by the fireball Doppler effect. Therefore it is expected that the rest frame radiation of many fireball sources might bear the Band function form, rather than a power law one (as adopted in Paper I). In this way, the effect of the radiation mechanism on the light curve might be different.

Following is the empirical radiation form of GRBs proposed by Band et al. (1993), the so-called Band function:

$$g_{0,\nu,B}(\nu_{0,\theta}) = \begin{cases} \left(\frac{\nu_{0,\theta}}{\nu_{0,p}}\right)^{1+\alpha_0} \exp\left[-(2+\alpha_0)\frac{\nu_{0,\theta}}{\nu_{0,p}}\right] & \left(\frac{\nu_{0,\theta}}{\nu_{0,p}} < \frac{\alpha_0-\beta_0}{2+\alpha_0}\right) \\ \left(\frac{\alpha_0-\beta_0}{2+\alpha_0}\right)^{\alpha_0-\beta_0} \exp(\beta_0-\alpha_0)\left(\frac{\nu_{0,\theta}}{\nu_{0,p}}\right)^{1+\beta_0} & \left(\frac{\nu_{0,\theta}}{\nu_{0,p}} \geq \frac{\alpha_0-\beta_0}{2+\alpha_0}\right) \end{cases}, \quad (54)$$

where subscript B represents the word Band, p stands for peak, α_0 and β_0 are the lower and

higher indexes, respectively. Typical values coming from statistical analysis, of the lower and higher indexes of the Band function, are $\alpha_0 = -1$ and $\beta_0 = -2.25$ (Preece et al. 1998, 2000), respectively. As mentioned above, the shape of rest frame spectra is not significantly changed by the expansion of fireballs. We take $g_{0,\nu}(\nu_{0,\theta}) = g_{0,\nu,B}(\nu_{0,\theta})$ and adopt $\alpha_0 = -1$ and $\beta_0 = -2.25$ to study the effect of the rest frame spectrum on the light curve of a local δ function pulse. Light curves of $C(\tau)$ determined by (35), emitted from the three emitting areas, calculated within the frequency range of $50 \leq \nu/\nu_{0,p} \leq 100$, for $\Gamma = 10$ and 100, are presented in Fig. 1, where $C(\tau)$ is normalized to the peak of the corresponding $C_0(\tau)$. The same features of cutoff tails are observed. Indicated by the figure, the impact of the rest frame radiation on the light curve can be obvious (here, the width of the pulse becomes smaller).

4 Count rate of general local pulses associated with different emitting areas in the fireball surface

In this section, we study the light curve of local pulses with a certain value of width, associated with different emitting areas in the fireball surface. A typical and very simple one is a local rectangle pulse, which will be studied in a much detail. Other forms of local pulses will also be studied. The limit of the time delay due to the constraint of the finite emission region of the three emitting areas discussed above will be taken into account.

4.1 The case of local rectangle pulses

To consider a local rectangle pulse we assume

$$I(t_\theta) = \begin{cases} I_0 & (t_{\theta,\min} \leq t_\theta \leq t_{\theta,\max}) \\ 0 & \text{and } (t_\theta < t_{\theta,\min} \text{ or } t_\theta > t_{\theta,\max}) \end{cases}, \quad (55)$$

where I_0 is a constant. From (55) we can come to

$$\tilde{I}(\tau_\theta) = \begin{cases} I_0 & (\tau_{\theta,\min} \leq \tau_\theta \leq \tau_{\theta,\max}) \\ 0 & \text{and } (\tau_\theta < \tau_{\theta,\min} \text{ or } \tau_\theta > \tau_{\theta,\max}) \end{cases}, \quad (56)$$

where, (14), (15), (16) and (23) are applied.

One finds from (26) and (27) that $\tau_{\theta,\min} \leq \tilde{\tau}_{\theta,\min}$ and $\tilde{\tau}_{\theta,\max} \leq \tau_{\theta,\max}$. With these relations, we come to the following by inserting (56) into (21):

$$C(\tau) = \frac{2\pi R_c^3 I_0 \int_{\tilde{\tau}_{\theta,\min}}^{\tilde{\tau}_{\theta,\max}} (1 + \beta\tau_\theta)^2 (1 - \tau + \tau_\theta) d\tau_\theta \int_{\nu_1}^{\nu_2} \frac{g_{0,\nu}(\nu_{0,\theta})}{\nu} d\nu}{hcD^2\Gamma^3(1 - \beta)^2(1 + k\tau)^2}. \quad (57)$$

This is the formula with which the count rate of a local rectangle pulse can be calculated.

To focus on how the local width of pulses affects the observed profile, here we ignore the possible effect from the spectrum and assume a δ function one:

$$g_{0,\nu}(\nu_{0,\theta}) = \delta(\nu_{0,\theta} - \nu_{0,0}) \quad (\nu_{0,\min} \leq \nu_{0,\theta} \leq \nu_{0,\max}), \quad (58)$$

with

$$\nu_{0,\min} < \nu_{0,0} < \nu_{0,\max}. \quad (59)$$

Corresponding to $\Gamma > 1$, $\beta > 0$ would be maintained and will be applied in the following. Applying (25), we can rewrite (58) as

$$\tilde{g}_{0,\nu}(\nu, \tau_\theta, \tau) = \delta\left[\frac{(1+k\tau)(1-\beta)\Gamma}{1+\beta\tau_\theta}(\nu - \nu_0)\right] \quad (\nu_{\min} \leq \nu \leq \nu_{\max}), \quad (60)$$

where

$$\tilde{g}_{0,\nu}(\nu, \tau_\theta, \tau) \equiv g_{0,\nu}[\nu_{0,\theta}(\nu, \tau_\theta, \tau)], \quad (61)$$

$$\nu_0 \equiv \frac{1 + \beta\tau_\theta}{\Gamma(1 - \beta)(1 + k\tau)}\nu_{0,0}, \quad (62)$$

$$\nu_{\min} \equiv \frac{1 + \beta\tau_\theta}{\Gamma(1 - \beta)(1 + k\tau)}\nu_{0,\min} \quad (63)$$

and

$$\nu_{\max} \equiv \frac{1 + \beta\tau_\theta}{\Gamma(1 - \beta)(1 + k\tau)}\nu_{0,\max}. \quad (64)$$

From (59) we find

$$\nu_{\min} < \nu_0 < \nu_{\max}, \quad (65)$$

where, (62), (63) and (64) are applied. According to the property of the δ function, we can rewrite (60) as

$$\tilde{g}_{0,\nu}(\nu, \tau_\theta, \tau) = \frac{1 + \beta\tau_\theta}{(1 + k\tau)(1 - \beta)\Gamma}\delta(\nu - \nu_0) \quad (\nu_{\min} \leq \nu \leq \nu_{\max}), \quad (66)$$

Suppose

$$\nu_1 < \nu_{\min} \quad (67)$$

and

$$\nu_{\max} < \nu_2. \quad (68)$$

Therefore,

$$\nu_1 < \nu_0 < \nu_2. \quad (69)$$

Replacing $g_{0,\nu}(\nu_{0,\theta})$ in (57) with $\tilde{g}_{0,\nu}(\nu, \tau_\theta, \tau)$ shown by (66) we obtain

$$C(\tau) = \frac{2\pi R_c^3 I_0}{\nu_0 h c D^2 \Gamma^4 (1-\beta)^3} \frac{\int_{\tilde{\tau}_{\theta,\min}}^{\tilde{\tau}_{\theta,\max}} (1 + \beta\tau_\theta)^3 (1 - \tau + \tau_\theta) d\tau_\theta}{(1 + k\tau)^3}, \quad (70)$$

Integrating (70) yields

$$C(\tau) = \frac{2\pi R_c^3 I_0}{5\nu_0 h c D^2 \Gamma^4 \beta^2 (1-\beta)^3} \left\{ [(1 + \beta\tilde{\tau}_{\theta,\max})^5 - (1 + \beta\tilde{\tau}_{\theta,\min})^5] (1 + k\tau)^{-3} - \frac{5}{4} (1 - \beta) [(1 + \beta\tilde{\tau}_{\theta,\max})^4 - (1 + \beta\tilde{\tau}_{\theta,\min})^4] (1 + k\tau)^{-2} \right\}, \quad (71)$$

where $\beta > 0$ is applied, and $\tilde{\tau}_{\theta,\min}$ and $\tilde{\tau}_{\theta,\max}$ are determined by (26) and (27), respectively. This is the formula for calculating the count rate of the local rectangle pulse which ignores the effect of spectra.

To make the plot of $C(\tau)$, we consider radiation from the three emitting areas discussed in last section: emitting areas 1, 2 and 3, which correspond to the whole fireball surface, the small area of $\theta \leq 1/\Gamma$ and that confined by (52), respectively. In the first case, (38) is applicable, and then from (26), (27) and (20) we get

$$\tilde{\tau}_{\theta,\min} = \max\{\tau_{\theta,\min}, \tau - 1\}, \quad (72)$$

$$\tilde{\tau}_{\theta,\max} = \min\{\tau_{\theta,\max}, \frac{\tau}{1-\beta}\}, \quad (73)$$

and

$$(1 - \beta)\tau_{\theta,\min} \leq \tau \leq 1 + \tau_{\theta,\max}, \quad (74)$$

respectively. In the second case, one should apply (49) and then gets

$$\tilde{\tau}_{\theta,\min} = \max\{\tau_{\theta,\min}, \frac{\tau - 1 + \cos \frac{1}{\Gamma}}{1 - \beta \cos \frac{1}{\Gamma}}\}, \quad (75)$$

$$\tilde{\tau}_{\theta,\max} = \min\{\tau_{\theta,\max}, \frac{\tau}{1-\beta}\}, \quad (76)$$

and

$$(1 - \beta)\tau_{\theta,\min} \leq \tau \leq 1 - \cos \frac{1}{\Gamma} + (1 - \beta \cos \frac{1}{\Gamma})\tau_{\theta,\max}. \quad (77)$$

In the third case, (52) would be applied, and then we obtain

$$\tilde{\tau}_{\theta,\min} = \max\{\tau_{\theta,\min}, \frac{\tau - 1 + \cos \frac{3}{2\Gamma}}{1 - \beta \cos \frac{3}{2\Gamma}}\} \quad (78)$$

$$\tilde{\tau}_{\theta,\max} = \min\{\tau_{\theta,\max}, \frac{\tau - 1 + \cos \frac{1}{2\Gamma}}{1 - \beta \cos \frac{1}{2\Gamma}}\}, \quad (79)$$

and

$$1 - \cos \frac{1}{2\Gamma} + (1 - \beta \cos \frac{1}{2\Gamma})\tau_{\theta,\min} \leq \tau \leq 1 - \cos \frac{3}{2\Gamma} + (1 - \beta \cos \frac{3}{2\Gamma})\tau_{\theta,\max}. \quad (80)$$

We employ the same Band function form of radiation with $\alpha_0 = -1$ and $\beta_0 = -2.25$, as adopted above, to illustrate profiles of $C(\tau)$ determined by (57), where $g_{0,\nu}(\nu_{0,\theta})$ would be replaced by $g_{0,\nu,B}(\nu_{0,\theta})$ shown in (54) and $\nu_{0,\theta}$ is related with ν by (25). Light curves arising from the three emitting areas, calculated within the frequency range of $50 \leq \nu/\nu_{0,p} \leq 100$, are presented in Fig. 2, where we take $2\pi R_c^3 I_0/hcD^2 = 1$, $\Gamma = 10$ and $\tau_{\theta,\min} = 0$, and adopt $\tau_{\theta,\max} = 0.2, 2$ and 20 , respectively. The figure shows explicitly a structure of FRED for the light curve arising from emitting area 1, suggesting that, such pulses can arise from a fireball surface when the local pulse involved lasts an interval of time (in contrast with it, there exists only an exponential decay phase in the light curve of a local δ function pulse, for which no rising phase can be seen). One finds that while the decay phase is due to the curvature effect, the rising portion of FRED pulses is produced by the width of the local pulse, which was already known (see, e.g., Paper I). (For a detailed analysis of the rising phase one could refer to Appendix B). One finds that the less the width of the local pulse, the narrower the observed rising phase. We suspect that, for many GRBs, FRED pulses observed might mainly be due to the expanding motion of fireballs. When taking different values of Γ , we find almost the same form of curves, suggesting that the character of FRED is a consequence of the expanding motion of fireballs as long as the motion is relativistic, no matter how large the Lorentz factor is. The cutoff tail feature is also observed in this figure (in the light curve arising from emitting area 2), with the longer the local pulse the less obvious the feature. When the local pulse is long enough, the cutoff tail feature would no more be visible, but instead, light curves arising from emitting area 2 in the decay phase would drop more rapidly than those from emitting area 1. In addition, for the patch moving along a direction with a small angle to the line of sight, the feature of the cutoff tail would not be visible when the local pulse is not very short (for extremely short local pulses, their light curves would approach to those of Fig. 1), and, interesting enough, the interval between the start and peak of its count rate is much larger than that associated with other two emitting areas. Plotting the light curves of (71), where the rest frame radiation form is ignored, we find almost the same result (the plot is omitted), suggesting that, to produce the profile of the light curves of the cases considered here, the rest frame radiation form does not play an important role (a more detailed discussion on the influence of the rest frame radiation form on the light curve, both for the magnitude and the profile, will be presented below).

4.2 The case of other forms of local pulses

Here we study if different forms of local pulses would lead to much different forms of expected light curves. In the following we consider several forms of local pulses other than the rectangle one.

First, let us consider a local pulse with an exponential rise and an exponential decay, which is written as

$$\tilde{I}(\tau_\theta) = I_0 \begin{cases} \exp(\frac{\tau_\theta - \tau_{\theta,0}}{\sigma}) & (\tau_{\theta,\min} \leq \tau_\theta \leq \tau_{\theta,0}) \\ \exp(-\frac{\tau_\theta - \tau_{\theta,0}}{\sigma}) & (\tau_{\theta,0} < \tau_\theta) \end{cases}. \quad (81)$$

This form of intensity belongs to the class of gradually shining and gradually dimming local pulses. [One could observe that, when $|\tau_\theta - \tau_{\theta,0}|/\sigma \ll 1$, intensity (81) would approach to that of linear functions.] Note that, since $1 + \beta\tau_\theta = R(t_\theta)/R_c > 0$ (see Appendix A), $\tau_\theta > -1/\beta$. That provides a constraint to the lower limit of τ_θ , i. e., $\tau_{\theta,\min} > -1/\beta$.

We employ the same Band function radiation form with $\alpha_0 = -1$ and $\beta_0 = -2.25$ to make the light curve. The count rate is determined by (21), where $g_{0,\nu}(\nu_{0,\theta})$ would be replaced by $g_{0,\nu,B}(\nu_{0,\theta})$ [see (54)], and $\nu_{0,\theta}$ is related with ν by (25). We also consider the three cases associated with emitting areas 1, 2, and 3, respectively. For emitting area 1, $\tilde{\tau}_{\theta,\min}$ and $\tilde{\tau}_{\theta,\max}$ would be determined by (72) and (73), respectively, while τ would be confined by (74); for emitting area 2, $\tilde{\tau}_{\theta,\min}$ and $\tilde{\tau}_{\theta,\max}$ would be calculated with (75) and (76), respectively, while τ would be confined by (77); for emitting area 3, $\tilde{\tau}_{\theta,\min}$ and $\tilde{\tau}_{\theta,\max}$ would be determined by (78) and (79), respectively, while the range of τ would be within that of (80). As the local emission time is limited by $\tau_\theta > -1/\beta$, it is impossible to take a negative infinity value of $\tau_{\theta,\min}$ and therefore the interval between $\tau_{\theta,0}$ and $\tau_{\theta,\min}$ must be limited. Here we assign $\tau_{\theta,0} = 10\sigma + \tau_{\theta,\min}$ so that the interval between $\tau_{\theta,0}$ and $\tau_{\theta,\min}$ would be large enough to make the rising part of the local pulse close to that of the exponential pulse.

Profiles of $C(\tau)$ determined by (21), of this local pulse, calculated within the frequency range of $50 \leq \nu/\nu_{0,p} \leq 100$, for the radiation emitted from the three emitting areas are also presented in Fig. 2, where we take $\Gamma = 10$, $\tau_{\theta,\min} = 0$, $2\pi R_c^3 I_0 / hcD^2 = 1$, and adopt $\sigma = 0.2, 2$ and 20 , respectively.

Shown in the figure, the structure of FRED is also observed, suggesting that the character of FRED is independent of the local structure of pulses. It is indeed a consequence of the expanding motion of fireballs. Different from those of the local rectangle pulses, the curves presented here are less sharp around the position of the peak count rate. A turn over, instead of a cutoff, tail

is observed in the light curves associated with this kind of local pulses, and the shorter the local pulse, the more obvious the turn over feature. For longer local pulses, the corresponding profiles seem to be the same (a direct comparison will be made below).

In addition, we consider three other local pulses. The first is a local pulse with an exponential rise

$$\tilde{I}(\tau_\theta) = I_0 \exp\left(\frac{\tau_\theta - \tau_{\theta,\max}}{\sigma}\right) \quad (\tau_{\theta,\min} \leq \tau_\theta \leq \tau_{\theta,\max}), \quad (82)$$

and the second is a local pulse with an exponential decay

$$\tilde{I}(\tau_\theta) = I_0 \exp\left(-\frac{\tau_\theta - \tau_{\theta,\min}}{\sigma}\right) \quad (\tau_{\theta,\min} \leq \tau_\theta), \quad (83)$$

and the third is a local pulse with a Gaussian form

$$\tilde{I}(\tau_\theta) = I_0 \exp\left[-\left(\frac{\tau_\theta - \tau_{\theta,0}}{\sigma}\right)^2\right] \quad (\tau_{\theta,\min} \leq \tau_\theta). \quad (84)$$

Among them, the first is a gradually shining and suddenly dimming local pulse, and the second is a suddenly shining and gradually dimming local pulse, while the third is a gradually shining and relatively fast dimming local pulse when $\tau_{\theta,\min} < \tau_{\theta,0}$.

We take the same parameters as those adopted in the case of local pulse (81) to study the light curves associated with these three local pulses, where for the first and third local pulses we assign $\tau_{\theta,\max} = 10\sigma + \tau_{\theta,\min}$ and $\tau_{\theta,0} = 10\sigma + \tau_{\theta,\min}$ respectively. The curves of $C(\tau)$ arising from the three emitting areas associated with these three local pulses are presented in Fig. 2 as well. We find that, light curves associated with local pulse (84) are similar to those associated with local pulse (81); in the case of local pulse (83), the cutoff or the turn over feature is visible only when the local pulse is short enough, otherwise it would no longer appear; for local pulse (82), light curves are even sharper than those associated with the rectangle local pulse, where the turn over feature is also observed, and is more obvious than that shown in the case of local pulse (81).

One can conclude from the figure that sudden dimming local pulses (either short or long) would give rise to sharp features of the light curves (see panels of the first and third rows in Fig. 2); gradually dimming local pulses would give birth to smooth light curves (see panels of the second and fourth rows in Fig. 2); relatively fast dimming local pulses would produce less smooth (or less sharp) light curves (see panels of the fifth row in Fig. 2). For relatively short light curves, the cutoff or the turn over tail feature would be obvious (see panels of the first column in Fig. 2).

It is noticed that, even though sudden dimming local pulses would give rise to sharp features of the light curves, suddenly shining local pulses would not. This must be due to the fact that the former would give up their roles to the curvature effect after the dimming begins, while the latter would not.

5 Impact of other factors on the profile of light curves

In this section, we will study impacts of other possible factors (other than different emitting areas discussed above) on the expected light curve of fireballs. How the width and structure of local pulses as well as the rest frame radiation form would affect the profile of light curves will be investigated. To focus on these effects, we consider here and in the late sections only the radiation emitted from the whole fireball surface (the so-called emitting area 1), for which, (38) would be applied.

5.1 Influence of the width of local pulses

The influence of the width of local pulses on the profile of light curves can be shown by plotting in a same figure various light curves corresponding to different widths of local pulses. In doing this, light curves should be normalized both in the magnitude and time scale so that they are visually comparable. In the following, for each curve, the magnitude of count rates would be normalized to a unit and the relative time, the variable, τ , would be re-scaled so that the peak count rate is located at $\tau = 0$ and the *FWHM* of the decay portion is located at $\tau = 0.2$.

To illustrate this effect in a more general manner, besides those local pulses discussed in last section, three other forms of local pulses are considered. The first is a local pulse with a power law rise and a power law decay which is assumed to be

$$\tilde{I}(\tau_\theta) = I_0 \left\{ \begin{array}{ll} \left(\frac{\tau_\theta - \tau_{\theta, \min}}{\tau_{\theta, 0} - \tau_{\theta, \min}} \right)^\mu & (\tau_{\theta, \min} \leq \tau_\theta \leq \tau_{\theta, 0}) \\ \left(1 - \frac{\tau_\theta - \tau_{\theta, 0}}{\tau_{\theta, \max} - \tau_{\theta, 0}} \right)^\mu & (\tau_{\theta, 0} < \tau_\theta \leq \tau_{\theta, \max}) \end{array} \right. . \quad (85)$$

[When $\mu = 1$, local pulse (85) would become a linear rise and a linear decay one.] For this local pulse we find $\tau_{\theta, FWHM1} = 2^{-1/\mu} \tau_{\theta, 0} + (1 - 2^{-1/\mu}) \tau_{\theta, \min}$ and $\tau_{\theta, FWHM2} = 2^{-1/\mu} \tau_{\theta, 0} + (1 - 2^{-1/\mu}) \tau_{\theta, \max}$. In this section, we consider only the case of $\mu = 2$. Thus, the *FWHM* of this local pulse would be $\Delta \tau_{\theta, FWHM} = (1 - 1/\sqrt{2})(\tau_{\theta, \max} - \tau_{\theta, \min})$, which leads to $\tau_{\theta, \max} = \Delta \tau_{\theta, FWHM} / (1 - 1/\sqrt{2}) + \tau_{\theta, \min}$. The second is a local pulse with a power law rise following

$$\tilde{I}(\tau_\theta) = I_0 \left(\frac{\tau_\theta - \tau_{\theta, \min}}{\tau_{\theta, \max} - \tau_{\theta, \min}} \right)^\mu \quad (\tau_{\theta, \min} \leq \tau_\theta \leq \tau_{\theta, \max}), \quad (86)$$

and the third is that with a power law decay which is written as

$$\tilde{I}(\tau_\theta) = I_0 \left(1 - \frac{\tau_\theta - \tau_{\theta,\min}}{\tau_{\theta,\max} - \tau_{\theta,\min}}\right)^\mu \quad (\tau_{\theta,\min} < \tau_\theta \leq \tau_{\theta,\max}). \quad (87)$$

In the case of $\mu = 2$, the relation of $\tau_{\theta,\max} = \Delta\tau_{\theta,FWHM}/(1 - 1/\sqrt{2}) + \tau_{\theta,\min}$ holds for the two latter local pulses. We observe that, the first belongs to the class of gradually shining and gradually dimming local pulses, the second is a gradually shining and suddenly dimming local pulse, and the third is a suddenly shining and gradually dimming local pulse.

We employ the same Band function radiation form with $\alpha_0 = -1$ and $\beta_0 = -2.25$ to make the light curve. The count rate is determined by (21), where $g_{0,\nu}(\nu_{0,\theta})$ would be replaced by $g_{0,\nu,B}(\nu_{0,\theta})$ [see (54)], and $\nu_{0,\theta}$ is related with ν by (25). We take $\Gamma = 10$ and $\tau_{\theta,\min} = 0$, and adopt $\Delta\tau_{\theta,FWHM} = 0.02, 0.2, 2$ and 20 , respectively, to make the profiles of the light curves of these local pulses, calculated within the frequency range of $50 \leq \nu/\nu_{0,p} \leq 100$ (see Fig. 3). For local pulse (85), $\tau_{\theta,0} = \tau_{\theta,\max}/2$ is adopted.

Shown in Fig. 3 are the normalized and re-scaled curves associated with various widths of local pulses for the five intensities studied in last section (where, except the magnitude and the time scale and the width of local pulses, all parameters are the same as those adopted in calculating the corresponding curves in Fig. 2) as well as the three intensities presented in this section. We find in Fig. 3 that, for suddenly dimming local pulses (see panels of the first column in the first, second and fourth rows), the shape, a concave curve, of the decay phase keeps to be the same for various values of the local pulse width (we therefore call it the standard decay curve); for a relatively fast dimming local pulse such as the Gaussian local pulse, the shape of the decay phase light curve slightly deviates from the standard form and keeps almost unchanged (see panel of the first column third row); for gradually dimming local pulses, the profile of the light curve in the decay phase varies with the local pulse width; for narrow local pulses, the width of the rising portion of the corresponding light curve, relative to that of the decay phase, is sensitive to the local pulse width, where the smaller the local pulse width the narrower the rising part of the light curve; for longer local pulses the relative width (relative to that of the decay part) of the rising portion of the light curve would no longer depend on the local pulse width, but instead, would keep to be unchanged. It is interesting that both convex and concave curves in the rising portion of the light curve could be observed in Fig. 3, which depend on the shape of local pulses.

To show in a much detail how the relative width of the rising portion, relative to that of the

decay phase, of light curves is affected by the local pulse width, we present Fig. 4, where, $FWHM1$ is the $FWHM$ of the rising portion, and $FWHM2$ is that of the decay phase. We find in this figure that the relative width, $FWHM1/FWHM2$, is sensitive to the local width as long as the latter is small enough. When the latter is sufficiently large, e.g. $\sigma = 1$, the former would remain unchanged, and in this situation, the two widths, $FWHM1$ and $FWHM2$, would be proportional to each other. This conclusion holds for any forms of local pulses. The upper limit of the sensitivity of the relative width to the local width differs for various forms of local pulses. For all kinds of local pulses, the value of $FWHM1/FWHM2$ would never exceed 1.3, which might be a criterion to check if a pulse arises from the emission of the whole fireball surface. Within the sensitivity range, the relative width would be uniquely related with the local width for any forms of the local pulse. In this situation, the former would be able to serve as an indicator of the latter.

Listed in Table 1 are the values of $FWHM1/FWHM2$ of the light curves of the eight local intensities analyzed in Fig. 4, for some typical values of the local width.

Note that, the words of “small width” and “large width” mentioned here are in terms of the relative time scale τ . As explained in section 2, even for a very thick shell which might produce a large time scale of a local pulse, if the size of the source is sufficiently large (such as the afterglow of GRBs) so that the dynamical time scale of the fireball which is defined with the fireball radius is large enough, when the ratio of the former time scale to the latter time scale is very small, the pulse would still be regarded as a short one and the ratio of the width of the rising portion of the light curve to that of the decay phase would be small, and, in this situation, the form of the local pulse employed to fit the light curve would not be important (see what discussed below). In particular, the profile of short pulses presented in Fig. 3 (i.e., the solid lines there) could be observed at very late epoches if the fireball model is applicable to a source and if the time scale of shocks is very small compared with the dynamical time scale of the fireball. In reverse, a shock creating very short time scale of local pulses could also lead to the profile of long pulses shown in Fig. 3 (e.g., the dot lines there) if the dynamical time scale of the fireball is small enough (such as in the period of the trigger time of bursts). A conclusion of these is that profiles of the curves in Fig. 3 could be observed in any periods of the light curves of GRBs if these sources can be described by the fireball model.

5.2 Influence of the shape of local pulses

To show how the shape of local pulses plays a role in producing the expected light curves of fireball sources we present Fig. 5. Displayed in this figure are the same curves of the panels of the first two rows of Fig. 3 (those of the panels of the last two rows are omitted due to the similarity), where light curves of different kinds, arising from a same local pulse width, are plotted in the same panel. We find that, the smaller the width of local pulses, the more similar the profile of light curves of various kinds of local pulses. When the local pulse is short enough (say $\sigma = 0.02$ or smaller), light curves arising from different forms of local pulses would not be distinguishable, for which, the shape of the light curve in the decay portion would be the same as those arising from suddenly dimming local pulses (the standard decaying form; see panels of the first column first and second rows of Fig. 3). This enables us to fit a light curve with a very short width of its rising portion, relative to that in the decay part, with any forms of local pulses, such as a local rectangle pulse, without causing a significant difference (in other words, one can fit such light curves quite satisfactorily without knowing the real form of the local pulse). This becomes one of the conclusions of this paper. Panels of the third and fourth columns of Fig. 5 show that, when the local pulse width is large enough, a certain kind of local pulses would produce a definite form of light curves and the profile of the curves would remain the same for different values of the local pulse width.

It is noticed that, the standard decaying curve is just the same as that produced by a very short local pulse, and for the latter, the decay phase must merely be due to the geometry of the fireball surface. Thus, the standard shape is associated with nothing but the pure curvature effect.

Since the decay phase of suddenly dimming local pulses (see solid lines in panels of the first and third rows of Fig. 5) bears the standard shape, the figure shows obviously that the decay curve of gradually dimming local pulses betrays the standard form in the manner that it is convex before $FWHM2$ and is concave after $FWHM2$ (see, e.g., solid lines in panels of the second, third and fourth columns of the second and fourth rows of Fig. 5). This manner will hold as long as the local pulse width is not very small (say, $\sigma = 0.2$ or larger).

5.3 Influence of the rest frame radiation form

Let us turn to study the impact of the rest frame radiation form on the expected light curve of fireballs. As a general radiation form observed, the Band function, for which, some sets of typical values of the indexes would represent certain mechanisms (see Band et al. 1993), will be employed in the following analysis. We will first investigate if different indexes would lead to a much different profile of light curves, and then will study how the evolution of the indexes is at work in producing the light curve.

The impact of indexes will be shown when light curves arising from the local pulses defined by (81) and (82) are plotted by taking different values of the indexes of the Band function. The previously adopted one, the Band function with $\alpha_0 = -1$ and $\beta_0 = -2.25$, will be compared with that of $\alpha_0 = -0.5$ and $\beta_0 = -3$ and that of $\alpha_0 = -1.5$ and $\beta_0 = -2$. Displayed in Fig. 6 are these curves. We find that, while the shapes of the light curves seem quite similar for different values of the indexes, their magnitudes differ obviously.

To tell how the shapes of the light curves are affected, we once more plot these curves in the manner adopted in plotting Fig. 3, where these light curves are normalized and their variables, τ , are re-scaled so that the peak count rate is located at $\tau = 0$ and the *FWHM* of the decay portion is located at $\tau = 0.2$. Presented in Fig. 7 are these normalized and re-scaled curves. It shows that, for relatively short local pulses, the profile of light curves would well keep its shape; for relatively longer local pulses, the profile would be mildly affected and the difference would be hardly detectable. We come to the conclusion that the profile is not significantly affected by the rest frame radiation form.

Another factor possibly affecting the profile of the light curve is the evolution of α_0 , which was often observed. Let us consider an evolution of the index ranging from $\alpha_0 = -0.5$ to $\alpha_0 = -1.5$. We once more study light curves arising from the local pulses defined by (81) and (82). For intensity (81), we assume $\alpha_0 = -1.5 + \exp[-(\tau_\theta - \tau_{\theta,\min})]$, and for intensity (82), we assume $\alpha_0 = -0.5 \exp[\ln 3 \times (\tau_\theta - \tau_{\theta,\min}) / (\tau_{\theta,\max} - \tau_{\theta,\min})]$. In this way, for both cases one would get $\alpha_0 = -0.5$ at the beginning of the local pulse and get $\alpha_0 = -1.5$ at the end. We calculate the count rate with these relations, where, other parameters are the same as those adopted in making Figs. 6 and 7. Similar results are obtained. The magnitude of the light curve is affected by the evolution of the index as well, as shown by those curves in Fig. 6. However, when plotting the

normalized and re-scaled light curve as done in Fig. 7, we come to the same conclusion. (The figures are omitted due to the similarity to Figs. 6 and 7.)

6 Application to some GRBs

According to the above analysis, we are aware that, if a gamma-ray burst is under the stage of fireballs, the profile of its light curve would be, or would be similar to, one of the curves of Fig. 3. If the width of the rising portion relative to that of the decay phase is very small, then the profile would be well fitted by one of the curves of the panels of the first column of Fig. 5, or by one close to those. In this situation, if the type of the corresponding local pulse is identified, then the local pulse width obtained by fit would be well determined since it is sensitive to the relative width observed for any types concerned (see Fig. 4). If the relative width is large enough, then the type (suddenly dimming or gradually dimming) of the corresponding local pulse would be well distinguished (see Fig. 5), although the local pulse width would no longer be determined (see Fig. 4).

Here we study the profile of light curves of several GRBs (GRB 910721, GRB 920925, GRB 930612, GRB 941026, GRB 951019, and GRB 951102B), which light curves are likely to be those of FRED pulses, trying to find out if the light curves could be represented by any of the curves discussed above, and if so, find out what could we obtain from the analysis.

Count rates of these sources are available in the web site of BATSE, where the presented counts are within the bin of $64ms$ for four energy channels (channel 1, $25 - 55kev$; channel 2, $55 - 110kev$; channel 3, $110 - 320kev$; channel 4, $> 320kev$). It has been already known that pulses of GRBs show a tendency to self-similarity across energy bands (see, e.g., Norris et al. 1996). Thus, we would study the count rate of only one of the channels. The one selected is channel 3, as the break energy of most GRBs could be found within this range (see Preece et al. 2000), and therefore count rates of this channel would be large enough for a statistical study. For each source, we assume its signal data covers the range of $t_{\min} \leq t \leq t_{\max}$, where $t_{\max} - t_{\min} = 2T_{90}$, and t_{\min} is at $T_{90}/2$ previous to the start of T_{90} . Data beyond this range, called sample 1, would be taken to find the fit of the background. These background data would first be smoothed with the DB3 wavelet (the first-class decomposition) with the MATLAB software, called sample 2, and then would be fitted with a linear function. This background fit would be applied to the signal interval and would be

taken as the background count rate there.

Data within the signal interval, called sample 3, subtracting the background counts would be taken as the signal data, called sample 4. First, sample 4 would be smoothed with the DB3 wavelet in the level of the third-class decomposition, and with these smoothed data, called sample 5, we would get primary values of the magnitude and position of the peak count rate, and then with these peak count rate parameters we would find the corresponding position of the *FWHM* in the decay phase. Second, sample 4 would be smoothed with the DB3 wavelet in the first-class decomposition level, and these smoothed data, called sample 6, would be normalized to the peak count rate and re-scaled to the positions of the peak and the *FWHM* (the former would be assigned to be 0 and the latter 0.2), called sample 7. We will compare the data of sample 7 with several theoretical curves discussed above, and among them the one that is the closest to the data would be selected. We will perform a fit to the data of sample 6 with the selected curve, where, the least square method would be used. When performing the fit, not only parameters of the curve, but also the magnitude as well as the time scale and the origin of time for the curve would be free. With the fitting curve, we would obtain the final values of the magnitude and position of the peak count rate and the *FWHM* in the decay phase, for sample 6. With these peak count rate and *FWHM* parameters, sample 6 would once more be normalized and re-scaled in the same way performed above, which is called sample 8. Data of sample 8 and the fitting curve will be presented in a same figure to show the result of the fit. The goodness of fit would be described by the statistics χ^2 which is defined by $\chi^2 \equiv \sum_{i=1}^n (C_{ob,i} - C_i)^2 / C_i$, where $C_{ob,i}$ and C_i are the observed and expected counts, respectively, within the i th bin, and n is the total number of bins. It is noticed that, in terms of statistics, the fluctuation of $C_{ob,i}$ must be due to both the signal and background counts. Sample 6 itself is not suitable to calculate χ^2 defined above. Therefore, in calculating the statistics, data of sample 6 plus the background fit would be employed to determine $C_{ob,i}$, and the fitting curve plus the same background fit would be employed to determine C_i (note that, in doing so, a zero value of C_i will no longer appears).

Let us study the count rates of GRB 930612 (#2387) in detail. The duration of GRB 930612 is $T_{90} = 41.984s$, and the start time of its T_{90} is $2.112s$. One finds $t_{\min} = -18.88s$ and $t_{\max} = 65.088s$.

First, let us check if there is a self-similarity across energy bands for this burst. This would be done when the profiles of the light curves of different channels are plotted in a same figure

and are compared. For this source, a FRED pulse light curve is visible in channels 1, 2, and 3 (in channel 4, the signal is hardly detectable). The fit of the background data for the three channels produces: $0.064C(t) = 181.2 - 0.043t$ (channel 1); $0.064C(t) = 138.6 - 0.039t$ (channel 2); $0.064C(t) = 125.2 - 0.053t$ (channel 3). With the method mentioned above, we find the primary value and position of the peak count rate for the three channels being 176.2 and 7.936s (channel 1), 261.5 and 5.888s (channel 2), and 294.6 and 4.416s (channel 3), respectively, and the position of the *FWHM* in the decay phase being 20.67s (channel 1), 17.73s (channel 2), and 13.12s (channel 3), respectively (where, when searching the primary value and position of the peak count rate, data of sample 4 of channel 1 are smoothed with the DB3 wavelet in the level of the fourth-class, instead of the third-class, decomposition, due to the much scatter of data in this channel). The normalized and re-scaled light curves of the burst in the three channels are shown in Fig. 8. We find that the profiles of the light curves in the three channels do not show an obvious different, indicating that the self-similarity character holds for this source.

Thus, we consider here only the case of channel 3. Comparing the data of sample 7 of channel 3 (see the pluses in the upper panel of Fig. 8) of this burst with those curves in Fig. 3, we find that the profile of the light curve arising from the local pulse of (83) with a sufficiently large local width is the most likely one accounting for the pulse observed. The light curve of this form of local pulses is therefore employed to perform a fit to sample 6. The main formula employed for performing the fit is equation (21), where for the rest frame radiation form we adopt the Band function (54). As the influence of the rest frame radiation form to the profile of light curves is insignificant (see Fig. 7) we adopt $\alpha_0 = -1$, $\beta_0 = -2.25$ and $\nu_{0,p} = 1keV$ to perform the fit. Since the profile of light curves is not sensitive to the Lorentz factor, as suggested in section 3, we adopt $\Gamma = 10$. In the same way, for the local pulse of (83) we take $\tau_{\theta, \min} = 0$. To meet the data observed, we assign $C_0 = 2\pi R_c^3 I_0 / hcD^2$ and $t = t_1\tau + t_0$, where C_0 , t_1 and t_0 are free parameters which would be determined by fit. The fitting parameters obtained with the least square method are listed in Table 2, where one finds that the probability of rejecting the null hypothesis is $P \ll 0.001$. This suggests that the profile of the light curve of GRB 930612 could indeed be accounted for by a fireball emitting with an exponentially decaying local pulse.

What could be determined from this analysis? As suggested in last section, the width of the local pulse is not sensitive to the profile of light curves when the former is large enough (see Figs.

4 and 5). For the fitting curve of this burst, we obtain $FWHM1/FWHM2 = 0.507$. According to Fig. 4, this value of $FWHM1/FWHM2$ is not sensitive to σ , and therefore the value of σ obtained by the fit above is not well determined. However, in this situation, the type (suddenly dimming or gradually dimming) of the corresponding local pulse is sensitive to the profile of light curves, and hence the light curve of GRB 930612 arising from a gradually dimming local pulse could be concluded, assuming that the source is undergoing the fireball stage.

It is noticed that, before performing the fit, the signal data are smoothed. Does the conclusion still hold if the data are not smoothed? To provide an answer to this, we simply calculate the χ^2 of the fitting curve with sample 4, and obtain $\chi^2 = 1281$. Taking 1308 as the number of degrees of freedom we find the corresponding probability, of rejecting the null hypothesis, as $P < 0.001$, indicating that the conclusion holds in this situation. But it shows that the goodness of fit owes much to the smooth of data (note that the smooth of data itself does not guarantee the goodness of fit without introducing a proper curve for the fit). The normalized and re-scaled fitting curve as well as the signal data without being smoothed are presented in Fig. 8 as well.

In the same way, count rates of channel 3 of GRB 910721 (#563), GRB 920925 (#1956), GRB 941026 (#3257), GRB 951019 (#3875) and GRB 951102B (#3892) are fitted, where we take the same values of α_0 , β_0 , $\nu_{0,p}$, Γ and $\tau_{\theta,\min}$ adopted above to perform the fits. Local pulse (83) is taken to make a fit to count rates for GRB 910721, while for GRB 941026 and GRB 951102B, local pulse (85) with $\mu = 1$ is adopted, and for GRB 920925 and GRB 951019, local pulse (86) with $\mu = 1$ is assumed. In determining the primary value and position of the peak count rate, sample 4 of GRB 941026 is smoothed with the DB3 wavelet in the level of the fourth-class decomposition, instead of the third-class decomposition adopted above, due to the much scatter of data (in this way, the position of the $FWHM$ in the decay phase can be better determined). For GRB 951019 and GRB 951102B, data of sample 4 are smoothed with the DB3 wavelet in the level of the second-class decomposition since they are less scatter.

Free parameters obtained by the fits are listed in Table 2 as well. We find for GRB 951102B that the probability, of rejecting the null hypothesis, is $P < 0.001$, while for the other four bursts, the probability is $P \ll 0.001$. It suggests that profiles of the light curve of these bursts could indeed be accounted for by the Doppler effect of fireballs when appropriate local pulses are assumed. Count rate light curves of sample 6 and the corresponding fitting curves of these sources are

presented in Fig. 9, where all the curves are normalized and re-scaled based on the value and the position of the peak count rate and the $FWHM$ position in the decay phase of the corresponding fitting curves, calculated in the same way adopted in Fig. 3. From these fitting curves we get $FWHM1/FWHM2 = 0.377, 0.819, 0.382, 0.416$ and 0.605 for GRB 910721, GRB 920925, GRB 941026, GRB 951019 and GRB 951102B, respectively. According to Fig. 4, parameters $\tau_{\theta,0}$ and $\tau_{\theta,max}$ obtained above are well determined for GRB 941026, GRB 951019 and GRB 951102B, while for GRB 910721 and GRB 920925, one can determine the ranges of $0.1 \leq \sigma \leq 1$ and $1 < \tau_{\theta,max}$, respectively.

7 Discussion and conclusions

The analysis in this paper is under the assumption that the curvature effect is important. Count rate formula used could not be applied to the cases in which the fireball surface is not (globally or locally) spherically symmetric, where the curvature effect is not at work. It should be pointed out that, as already known, the profile of the pulses observed could be well represented by various pulse functions and then the curvature effect is not a unique mechanism to account for it. The analysis of the profile of pulses alone is not sufficient to tell if the curvature effect is important. To find an answer to this, other efforts should be made.

As shown above, the profile of pulses of fireball sources is not sensitive to the rest frame radiation form, and based on this we are able to perform fits to the light curves of several bursts under the assumption that they are undergoing the fireball stage. However, as suggested by (21), count rates of different energy channels could be described by a single formula. Could one perform fits to the four channel light curves observed by BATSE with (21)? The answer is yes if all physical parameters of a source are known. We find that, to account for different channel light curves, the rest frame radiation form plays an important role. As the corresponding rest frame radiation parameters are not available for us, we could not perform a further investigation on the fits to the sources discussed above.

Nevertheless, it would make sense if only showing how equation (21) is at work when several channel light curves of a source are concerned. Here, let us try to fit the four channel light curves of GRB 951019 when adopting various sets of the rest frame radiation parameters. The method is the same as that adopted in last section, except that we deal with four channels, instead of one.

When taking $\alpha_0 = -1$, $\beta_0 = -2.25$, $\Gamma = 100$, $\tau_{\theta,\min} = 0$, $\tau_{\theta,\max} = 0.518$ and $\mu = 1$, we obtain $\nu_{0,p} = 1.06\text{keV}$, $C_0 = 4.91$, $t_1 = 28800$ and $t_0 = -0.583$, which leads to $\chi^2 = 1186$ (with the number of degrees of freedom being 1044). The probability is $P = 0.00191$. When adopting $\alpha_0 = -0.5$, $\beta_0 = -3.5$, $\Gamma = 100$, $\tau_{\theta,\min} = 0$, $\tau_{\theta,\max} = 0.518$ and $\mu = 1$, we get $\nu_{0,p} = 0.907\text{keV}$, $C_0 = 11.1$, $t_1 = 27600$ and $t_0 = -0.562$, which produces $\chi^2 = 779.2$ (the number of degrees of freedom is the same). The corresponding probability is $P \ll 0.001$. (When allowing α_0 and β_0 to be free, the fit will be slightly improved.) Presented in Fig. 10 are the fitting curves of the second case, together with the observed data of the four channel light curves of the source. It shows that, different channel light curves of a burst could indeed be accounted for by a single formula. Relations between them might mainly be due to the Doppler effect of fireballs. The *FWHM* of the fitting curves of the second case are related with energy by a power law of $\log(FWHM/s) = 0.38 - 0.24 \log(E/\text{keV})$. The index, -0.24 , is different from -0.4 which was obtained previously (see, e.g., Fenimore et al. 1995). Note that, if -0.24 could be convinced (e.g., when the adopted rest frame radiation indexes are true), it is from a single burst, but -0.4 arises from the sum of the *FWHM* of the individual sources of a sample and these widths depend on the distribution of the rest frame radiation parameters.

Although if the power law index of GRB 951019 is -0.24 is still an open question, a power law relationship between the width and energy holds for this burst would be true, which is obviously displayed in Fig. 10. Under the theory of the Doppler effect of fireballs, this phenomenon is naturally explained. While photons emitted from the small area of the fireball surface with $\theta \sim 0$ would be observed in higher energy channels due to the Doppler effect, those radiated from the larger area of the fireball surface must be observed in lower energy channels, and the latter must last a much longer time due to the geometric delay. This, we suspect, might become a useful approach to check if the curvature effect is at work for any bursts concerned.

As can be deduced from previous studies (see, e.g., Paper I), due to the Doppler effect of fireballs, neglecting the area of $\theta > 1/\Gamma$ would lead a light curve with a cutoff tail, or a turn over, in its decay phase, which we call a cutoff tail problem. This feature would be obvious when the local pulse is short enough, and under this circumstance, the feature would become a criterion to pick out those sources emitted from the area of $\theta < 1/\Gamma$, from others (note that, as the count rate at $\theta = 1/\Gamma$ is a quarter of the peak, the feature would be obviously observable). When the

local pulse is long, the cutoff tail, or the turn over, feature would be less obvious and even be no more visible. For the case of a patch moving along the direction of $\theta \sim 1/\Gamma$, the light curve also exhibits the feature of cutoff tails when the local pulse is short enough (see Fig. 1). Compared with that of the patch moving towards the observer, its light curve lasts a much longer time, while the amplitude becomes much smaller. When the local pulse lasts a sufficient interval of time, the cutoff tail, or the turn over, feature would no longer be visible for this patch, but instead, a full structure of FRED would be observed (see Fig. 2). As noted by Ryde and Svensson (2002), there are some bursts that their light curves have a sudden change, going into a more rapid decay. In terms of the curvature effect, this turn over feature could be interpreted as the light curves coming from the radiation of hot spots.

As shown in Fig. 4, when the local pulse width is small enough, the ratio of the width of the light curve in the rising portion to that in the decay phase would be sensitive to it, and in this situation, the ratio could be well determined by fit. However, when the local pulse width is large, the ratio would remain unchanged and the two quantities are no more uniquely related and then this method would fail.

Replacing $\Gamma = 10$ with $\Gamma = 100$ when calculating some curves discussed above, we find that the profile of light curves of fireballs is not significantly affected by the Lorentz factor, suggesting that conclusions referring to profiles would be maintained when different values of Γ within this range are considered. Thus, the character of FRED as a consequence of the Doppler effect of fireballs is independent of the Lorentz factor as long as the factor is large enough to represent a relativistic motion. In addition, as shown in Figs. 3 and 6, the character could result from any forms of local pulses and from any rest frame radiation forms.

The interval $\Delta\tau_{pb}$ between the observed beginning and the peak of the light curve of a local rectangle pulse is proportional to the local width of the pulse (see Appendix B for a detailed analysis). For a large value of the Lorentz factor, the peak count rate C_p of the light curve of local rectangle pulses would be proportional to $1/\Gamma^4\beta^2(1-\beta)^3$. With the two quantities we get

$$\frac{C_p}{\Delta\tau_{pb}} \propto \frac{\Gamma^4}{\Delta\tau_\theta} \quad (\Gamma \gg 1). \quad (88)$$

It indicates that the slope of the up rising part of an FRED pulse, if it arises from a local pulse with a constant emission, would be very sensitive to the Lorentz factor and be sensitive to the width of the local pulse as well. Therefore, quantity $C_p/\Delta\tau_{pb}$ of pulses might be useful for detecting the

expanding speed of GRBs.

As is shown above, our analysis focuses on the model of fireballs which are highly symmetric and expand relativistically. However, since the derivation does not rely on any assumptions of the Lorentz factor, the basic formulas (those in section 2) are applicable to sub-relativistic cases as well as non-relativistic cases, as long as the objects concerned are highly symmetric and are isotropically expanding. In our derivation, the thickness of the outer shell is not taken into account. This does not matter. In the analysis, the concept of the surface intensity is employed. Any radiation from the shell must pass through the surface and at any time there is a unique value of radiation passing through it, and this is the quantity defined as the surface intensity. In this way, all radiations from or behind the shell are included.

It should be noticed that the formula presented in this paper is applicable to the radiation emitted from small areas such as $\theta \leq 1/\Gamma$ as long as the areas concerned are locally highly symmetric. If all GRBs are beamed, the discussion of the radiation emitted from the whole fireball surface would become meaningless. However, since count rate light curves of all the GRBs observed so far vary enormously, we suspect that there might be various models accounting for all of these objects. Due to the great output rate of the radiation observed, many GRBs would undergo the fireball stage and some of them might probably be observed when they remain in this stage. For a burst arising from the collapse of some massive objects, the consequent fireball could become highly symmetric. The emitting area would be the whole fireball surface when the radiation occurs before the fireball shell is distorted, while it would be a patch (or a hot spot) when a short inner jet hits the outer shell.

We suspect that, if during some period of time, continuous explosion inside the fireball lasts an interval of time and its intensity keeps unchanged, then the local pulse would be approximated by a rectangle one, as long as the cooling time scale is short enough. Under the situation that the radiation seeds (e.g., electrons) are distributed within the outer shell geometrically with a Gaussian form and the inner shock occurred is quite strong so that both inner and outer electrons gain the same amount of energy from the shock, a local Gaussian pulse might be produced (also, the cooling time scale is assumed to be short enough).

In fitting the count rates of the six GRBs, we have very few free parameters for each of them. It is plain that, when allowing other parameters such as the indexes of the Band function to be

variable, one would get much better fits. However, in last section we focus on the question that if there are any GRBs that the profiles of their count rate light curves can be described by the count rate formula provided. If the formula can explain the observed profiles when adopting some simple forms of the intensity of local pulses and some certain values of the corresponding quantities (in fact, as the χ^2 shows, this is true), our task will be reached. As pointed out above, the profile of count rate light curves of fireballs is not sensitive to the Lorentz factor as long as the factor is large enough to represent a relativistic motion. Thus, adopting $\Gamma = 10$ is not fatal for the goodness of fit of the six GRBs (one can check that adopting other values of Γ would also produce well fits for these sources). Note that, in fitting the count rates of these GRBs, the cosmological effect is ignored due to the lack of the knowledge of redshifts. While the change of the magnitude of the light curves when taking into account the cosmological effect can be absorbed into the magnitude itself, the frequency shifting of the effect would affect the values of the quantities associated with τ . However, the cosmological factor which is $1 + z$ can be absorbed into these quantities as well, and in this way the fitting curves in Figs. 8 and 9 will not be affected.

As is mentioned above, the count rate formula presented in this paper is derived in detail which does not rely on any approximately valued quantities or estimated methods. Therefore it would be generally applicable. When some factors are ignored, it will come to previous formulas such as those presented in Papers I and II. A constraint of applying the formula is that the object concerned must be one emitted within a locally highly symmetric area which move outwards isotropically relative to the center of the object, such as a cone expanding towards to the observer. Due to the vast difference between various light curves of GRBs observed, we believe that the shape of the light curves must vary significantly from source to source, and for many GRBs the above constraint might not be satisfied. Therefore, to study statistical properties of GRBs, it would be better to employ empirical or semi-empirical functions such as those presented in Norris et al. (1996) and Kocevski et al. (2003). Compared with those empirical functions, the formula presented in this paper is more suitable to be applied to individual sources when their count rate light curves are seen to be likely affected by the curvature effect (e.g., if there exists a structure of FRED in all the well separated pulses of the sources).

Acknowledgments

This work was supported by the Special Funds for Major State Basic Research Projects (“973”) and National Natural Science Foundation of China (No. 10273019).

Appendix A. Relation between the peak count rate and the width of $C_0(\tau)$

Here, we employ the concept of *FWHM* to describe the width of $C_0(\tau)$.

One can verify from (36) that the maximum value of $C_0(\tau)$ would be obtained when $\tau \rightarrow (1 - \beta)\tau_{\theta,0}$. Let

$$C_{0,p} \equiv C_0[\tau \rightarrow (1 - \beta)\tau_{\theta,0}]. \quad (A1)$$

Then, from (36) we obtain

$$C_{0,p} = \frac{1 + \beta\tau_{\theta,0}}{\Gamma^3(1 - \beta)^2}. \quad (A2)$$

Applying (A2), when $\beta > 0$, one can obtain from (36) that

$$\tau_H = \frac{-(1 + k + \beta\tau_{\theta,0}) + (1 + \beta\tau_{\theta,0})\sqrt{k^2 + (1 + k)^2}}{k^2}, \quad (A3)$$

where

$$C_0(\tau = \tau_H) = \frac{C_{0,p}}{2}. \quad (A4)$$

Therefore, the width, described by the concept of *FWHM*, of the light curve of the local δ function pulse would be

$$\Delta\tau_{FWHM} = \tau_H - (1 - \beta)\tau_{\theta,0} = \frac{(\Gamma - \sqrt{\Gamma^2 - 1})(\sqrt{2\Gamma^2 - 1} - \Gamma)}{\Gamma^2 - 1}(1 + \beta\tau_{\theta,0}). \quad (A5)$$

From (39) we learn that the interval of the observable time of the local δ function pulse is

$$\Delta\tau = 1 + \tau_{\theta,0} - (1 - \beta)\tau_{\theta,0} = 1 + \beta\tau_{\theta,0}. \quad (A6)$$

According to Paper III, the radius of the fireball at time t_θ can be determined by

$$R(t_\theta) = (t_\theta - t_c)\beta c + R_c. \quad (A7)$$

Inserting (32) into (A7) we find

$$1 + \beta\tau_{\theta,0} = \frac{R(t_{\theta,0})}{R_c}. \quad (A8)$$

Thus, $\Delta\tau$ represents, in a relative term, the time scale of the real size of the fireball at the corresponding emission time, $t_{\theta,0}$. Applying (A8) we get from (A5) that

$$\Delta\tau_{FWHM} = \frac{(\Gamma - \sqrt{\Gamma^2 - 1})(\sqrt{2\Gamma^2 - 1} - \Gamma)}{\Gamma^2 - 1} \frac{R(t_{\theta,0})}{R_c}. \quad (A9)$$

From (A2) one finds

$$C_{0,p} = \frac{1}{\Gamma(\Gamma - \sqrt{\Gamma^2 - 1})^2} \frac{R(t_{\theta,0})}{R_c}, \quad (A10)$$

where, (A8) is applied. Combining (A9) and (A10) we get

$$C_{0,p} = \frac{\Gamma^2 - 1}{\Gamma(\Gamma - \sqrt{\Gamma^2 - 1})^3(\sqrt{2\Gamma^2 - 1} - \Gamma)} \Delta\tau_{FWHM}. \quad (A11)$$

This is the relation between the peak count rate and the width of $C_0(\tau)$.

Inserting (A2) into (36) yields

$$\frac{C_0(\tau)}{C_{0,p}} = \frac{(\frac{\Delta\tau}{\beta} - \frac{1}{k} - \tau)\Delta\tau}{(1 + k\tau)^2}, \quad (A12)$$

where (A6) is applied. With this, the ratio of a certain count rate to the peak count rate of $C_0(\tau)$ for any observation time is determined. An important application of this is to consider the case of $\theta_{\max} = 1/\Gamma$, for which we obtain the maximum value of τ from (51). Applying this value to (A12) and assuming $\Gamma \gg 1$ we get

$$C_0(\tau|_{\theta=1/\Gamma}) \simeq \frac{C_{0,p}}{4}. \quad (A13)$$

Appendix B. Peak count rate of the light curve of local rectangle pulses ignoring the rest frame spectral form

Here we present a detailed study on the peak count rate of the light curve of a local rectangle pulse with its rest frame spectrum being a δ function form, for which the count rate is determined by (71).

We consider the case of the whole fireball surface for which (38) is applied. In this case (72), (73) and (74) are applicable. From (74) we find that, if

$$(1 - \beta)\tau_{\theta, \max} < 1 + \tau_{\theta, \min}, \quad (B1)$$

there will be three ranges of τ : $I_I \equiv \{(1 - \beta)\tau_{\theta, \min} \leq \tau \leq (1 - \beta)\tau_{\theta, \max}\}$, $I_{II} \equiv \{(1 - \beta)\tau_{\theta, \max} \leq \tau \leq 1 + \tau_{\theta, \min}\}$, and $I_{III} \equiv \{1 + \tau_{\theta, \min} \leq \tau \leq 1 + \tau_{\theta, \max}\}$. If

$$1 + \tau_{\theta, \min} < (1 - \beta)\tau_{\theta, \max}, \quad (B2)$$

there will be three other ranges of τ : $II_I \equiv \{(1 - \beta)\tau_{\theta, \min} \leq \tau \leq 1 + \tau_{\theta, \min}\}$, $II_{II} \equiv \{1 + \tau_{\theta, \min} \leq \tau \leq (1 - \beta)\tau_{\theta, \max}\}$, and $II_{III} \equiv \{(1 - \beta)\tau_{\theta, \max} \leq \tau \leq 1 + \tau_{\theta, \max}\}$.

One can check that, in range I_I , $\tilde{\tau}_{\theta, \min} = \tau_{\theta, \min}$ and $\tilde{\tau}_{\theta, \max} = \tau/(1 - \beta)$, and then we get from (71) that

$$C(\tau) = \frac{2\pi R_c^3 I_0}{5\nu_0 hc D^2 \Gamma^4 \beta^2 (1 - \beta)^3} \left\{ \frac{(5\beta - 1)(1 + k\tau)^2}{4} + \frac{5(1 - \beta)(1 + \beta\tau_{\theta, \min})^4}{4(1 + k\tau)^2} - \frac{(1 + \beta\tau_{\theta, \min})^5}{(1 + k\tau)^3} \right\}; \quad (B3)$$

in range I_{II} , $\tilde{\tau}_{\theta, \min} = \tau_{\theta, \min}$ and $\tilde{\tau}_{\theta, \max} = \tau_{\theta, \max}$, and then we get

$$C(\tau) = \frac{2\pi R_c^3 I_0}{5\nu_0 hc D^2 \Gamma^4 \beta^2 (1 - \beta)^3} \left\{ \frac{(1 + \beta\tau_{\theta, \max})^5 - (1 + \beta\tau_{\theta, \min})^5}{(1 + k\tau)^3} - \frac{5[(1 + \beta\tau_{\theta, \max})^4 - (1 + \beta\tau_{\theta, \min})^4]}{4(1 - \beta)^{-1}(1 + k\tau)^2} \right\}; \quad (B4)$$

in range I_{III} , $\tilde{\tau}_{\theta, \min} = \tau - 1$ and $\tilde{\tau}_{\theta, \max} = \tau_{\theta, \max}$, and then we get

$$C(\tau) = \frac{2\pi R_c^3 I_0}{5\nu_0 hc D^2 \Gamma^4 \beta^2 (1 - \beta)^3} \left\{ \frac{(1 + \beta\tau_{\theta, \max})^5}{(1 + k\tau)^3} - \frac{5(1 - \beta)(1 + \beta\tau_{\theta, \max})^4}{4(1 + k\tau)^2} + \frac{(1 - \beta)^5(1 + k\tau)^2}{4} \right\}; \quad (B5)$$

in range II_I , $\tilde{\tau}_{\theta, \min} = \tau_{\theta, \min}$ and $\tilde{\tau}_{\theta, \max} = \tau/(1 - \beta)$, then we get (B3); in range II_{II} , $\tilde{\tau}_{\theta, \min} = \tau - 1$ and $\tilde{\tau}_{\theta, \max} = \tau/(1 - \beta)$, and then we get

$$C(\tau) = \frac{2\pi R_c^3 I_0}{5\nu_0 hc D^2 \Gamma^4 \beta^2 (1 - \beta)^3} \frac{5\beta - 1 + (1 - \beta)^5}{4} (1 + k\tau)^2; \quad (B6)$$

in range II_{III} , $\tilde{\tau}_{\theta, \min} = \tau - 1$ and $\tilde{\tau}_{\theta, \max} = \tau_{\theta, \max}$, and then we get (B5).

Here, we pay our attention to relativistic motions, and hence we assume

$$\beta > \frac{3}{5} \quad (B7)$$

in the following analysis.

a) In the case of $(1 - \beta)\tau_{\theta, \max} < 1 + \tau_{\theta, \min}$, we have (B3) in range I_I , (B4) in range I_{II} and (B5) in range I_{III} . Differentiating (B3), (B4), and (B5) we obtain

$$= \frac{\pi R_c^3 I_0}{5\nu_0 hc D^2 \Gamma^4 \beta (1 - \beta)^4} \frac{\frac{dC(\tau)}{d\tau}}{(1 + k\tau)^4} \left\{ [(5\beta - 1)(1 + k\tau)^4 - 5(1 - \beta)(1 + \beta\tau_{\theta, \min})^4](1 + k\tau) + 6(1 + \beta\tau_{\theta, \min})^5 \right\}, \quad (B8)$$

$$= \frac{\pi R_c^3 I_0}{5\nu_0 hc D^2 \Gamma^4 \beta (1-\beta)^4} \frac{\frac{d}{d\tau} C(\tau)}{(1+k\tau)^4} \{5[(1+\beta\tau_{\theta,\max})^4 - (1+\beta\tau_{\theta,\min})^4](1-\beta)(1+k\tau) - 6[(1+\beta\tau_{\theta,\max})^5 - (1+\beta\tau_{\theta,\min})^5]\}, \quad (B9)$$

and

$$= \frac{\pi R_c^3 I_0}{5\nu_0 hc D^2 \Gamma^4 \beta (1-\beta)^4} \frac{\frac{d}{d\tau} C(\tau)}{(1+k\tau)^4} \{[(1-\beta)^4(1+k\tau)^4 + 5(1+\beta\tau_{\theta,\max})^4](1-\beta)(1+k\tau) - 6(1+\beta\tau_{\theta,\max})^5\}, \quad (B10)$$

respectively.

One finds $\beta\tau_{\theta,\min} \leq k\tau \leq \beta\tau_{\theta,\max}$ in range I_I , $(1-\beta)(1+k\tau) \leq 1 + \beta\tau_{\theta,\min}$ in range I_{II} , and $(1-\beta)(1+k\tau) \leq (1 + \beta\tau_{\theta,\max})$ in range I_{III} . Therefore,

$$(5\beta - 1)(1+k\tau)^4 - 5(1-\beta)(1+\beta\tau_{\theta,\min})^4 \geq 2(5\beta - 3)(1+\beta\tau_{\theta,\min})^4 > 0 \quad (\tau \in I_I), \quad (B11)$$

$$5[(1+\beta\tau_{\theta,\max})^4 - (1+\beta\tau_{\theta,\min})^4](1-\beta)(1+k\tau) - 6[(1+\beta\tau_{\theta,\max})^5 - (1+\beta\tau_{\theta,\min})^5] \leq -[(1+\beta\tau_{\theta,\max})^4 - (1+\beta\tau_{\theta,\min})^4](1+\beta\tau_{\theta,\min}) \leq 0 \quad (\tau \in I_{II}), \quad (B12)$$

$$[(1-\beta)^4(1+k\tau)^4 + 5(1+\beta\tau_{\theta,\max})^4](1-\beta)(1+k\tau) - 6(1+\beta\tau_{\theta,\max})^5 \leq 0 \quad (\tau \in I_{III}). \quad (B13)$$

In this case, $dC(\tau)/d\tau > 0$ in range I_I , $dC(\tau)/d\tau \leq 0$ in range I_{II} , and $dC(\tau)/d\tau \leq 0$ in range I_{III} . Hence, the peak of $C(\tau)$ must be located at the upper limit of τ in range I_I . That is

$$C_{I,p} = C[\tau = (1-\beta)\tau_{\theta,\max}] = \frac{2\pi R_c^3 I_0}{5\nu_0 hc D^2 \Gamma^4 \beta^2 (1-\beta)^3} \left\{ \frac{(1+\beta\tau_{\theta,\max})^5 - (1+\beta\tau_{\theta,\min})^5}{(1+\beta\tau_{\theta,\max})^3} - \frac{5(1-\beta)[(1+\beta\tau_{\theta,\max})^4 - (1+\beta\tau_{\theta,\min})^4]}{4(1+\beta\tau_{\theta,\max})^2} \right\}. \quad (B14)$$

b) In the case of $1 + \tau_{\theta,\min} < (1-\beta)\tau_{\theta,\max}$, we have (B3) in range II_I , (B6) in range II_{II} and (B5) in range II_{III} . Differentiating (B3) and (B5) we obtain (B8) and (B10), respectively. Differentiating (B6) we get

$$\frac{d}{d\tau} C(\tau) = \frac{\pi R_c^3 I_0}{5\nu_0 hc D^2 \Gamma^4 \beta (1-\beta)^4} [(1-\beta)^5 + 5\beta - 1](1+k\tau). \quad (B15)$$

We find $\beta\tau_{\theta,\min} \leq k\tau$ in range II_I and $(1-\beta)(1+k\tau) \leq (1 + \beta\tau_{\theta,\max})$ in range II_{III} . In the same way, one reaches $dC(\tau)/d\tau > 0$ in range II_I and $dC(\tau)/d\tau \leq 0$ in range II_{III} . Since $\beta > 3/5$, we find that

$$(1-\beta)^5 + 5\beta - 1 > (1-\beta)^5 + 2 > 0. \quad (B16)$$

Hence, $dC(\tau)/d\tau > 0$ in range II_{II} . Therefore, the peak of $C(\tau)$ must be located at the upper limit of τ in range II_{II} . That is

$$C_{II,p} = C[\tau = (1-\beta)\tau_{\theta,\max}] = \frac{2\pi R_c^3 I_0}{5\nu_0 hc D^2 \Gamma^4 \beta^2 (1-\beta)^3} \frac{[(1-\beta)^5 + 5\beta - 1](1+\beta\tau_{\theta,\max})^2}{4}. \quad (B17)$$

As shown above, when $\beta > 3/5$, the position of the peak count rate of the light curve of local rectangle pulses would be located at $\tau = (1 - \beta)\tau_{\theta,\max}$. Therefore, according to (74), the interval between the beginning and the peak of the pulse would be

$$\Delta\tau_{pb} \equiv (1 - \beta)\tau_{\theta,\max} - (1 - \beta)\tau_{\theta,\min} = (1 - \beta)(\tau_{\theta,\max} - \tau_{\theta,\min}). \quad (B18)$$

Let

$$\Delta\tau_{\theta} \equiv \tau_{\theta,\max} - \tau_{\theta,\min}. \quad (B19)$$

One finds

$$\Delta\tau_{pb} = (1 - \beta)\Delta\tau_{\theta}. \quad (B20)$$

It suggests that the interval between the observed beginning and the peak of the light curve of a local rectangle pulse is proportional to the local width of the pulse. For a same kind of local rectangle pulses, $\Delta\tau_{pb}$ would become an indicator of the Lorentz factor of the expanding fireball.

From (B20) one finds that, when $\Delta\tau_{\theta} \rightarrow 0$, $\Delta\tau_{pb} \rightarrow 0$. The profile would approach that of local δ function pulses.

From (B14) and (B17) we observe that, when $\Gamma \gg 1$, the peak of the count rate would be proportional to $1/\Gamma^4\beta^2(1 - \beta)^3$. Let C_p be the observed peak count rate of a pulse. One can check that

$$\frac{C_p}{\Delta\tau_{pb}} \propto \frac{\Gamma^4}{\Delta\tau_{\theta}} \quad (\Gamma \gg 1). \quad (B21)$$

This indicates that the slope of the up rising part of an FRED pulse, if it can be described by the light curve of a local rectangle pulse, would be very sensitive to the Lorentz factor and be sensitive to the width of the local pulse as well.

Quantities $\Delta\tau_{pb}$ and $C_p/\Delta\tau_{pb}$ of pulses might be useful for detecting the expanding speed of GRBs, so long as the pulses can be described by the light curve of local rectangle pulses.

REFERENCES

- Band, D., et al. 1993, ApJ, 413, 281
- Fenimore, E. E., Epstein, R. I., and Ho, C. 1993, A&AS, 97,59
- Fenimore, E. E., in't Zand, J. J. M., Norris, J. P., Bonnell, J. T., and Nemiroff, R. J.
1995, ApJ, 448, L101
- Fenimore, E. E., Madras, C. D., and Nayakshin, S. 1996, ApJ, 473, 998 (Paper I)
- Fishman, G. J., et al. 1994, ApJS, 92, 229
- Ford, L. A., Band, D. L., Mattesou, J. L., et al. 1995, ApJ, 439, 307
- Goodman, J. 1986, ApJ, 308, L47
- Hailey, C. J., Harrison, F. A., and Mori, K. 1999, ApJ, 520, L25
- Kocevski, D., Ryde, F., and Liang, E. 2003, ApJ, 596, 389
- Krolik, J. H., and Pier, E. A. 1991, ApJ, 373, 277
- Mészáros, P., and Rees, M. J. 1998, ApJ, 502, L105
- Norris, J. P., Nemiroff, R. J., and Bonnell, J. T. et al. 1996, ApJ, 459, 393
- Paczynski, B. 1986, ApJ, 308, L43
- Preece, R. D., Pendleton, G. N., Briggs, M. S., et al. 1998, ApJ, 496, 849
- Preece, R. D., Briggs, M. S., Mallozzi, R. S., et al. 2000, ApJS, 126, 19
- Qin, Y.-P. 2002, A&A, 396, 705 (Paper III)
- Qin, Y.-P. 2003, A&A, 407, 393
- Ryde, F., and Petrosian, V. 2002, ApJ, 578, 290 (Paper II)
- Ryde, F., and Svensson, R., ApJ, 566, 210
- Schaefer, B. E., Teegaeden, B. J., Fantasia, S. F., et al. 1994, ApJS, 92, 285

Table 1: Typical values of $FWHM1/FWHM2$ withdrawn from Fig. 4

σ (or $\tau_{\theta,max}, \Delta\tau_{\theta,FWHM}$)	rect	erd	er	ed	Gau	prd	pr	pd
0.01	0.02	0.11	0.03	0.12	0.07	0.06	0.03	0.09
0.10	0.20	0.28	0.14	0.34	0.25	0.31	0.22	0.42
1.00	1.07	0.35	0.24	0.44	0.37	0.58	0.57	0.79
10.0	1.23	0.36	0.25	0.51	0.39	0.63	0.67	0.88

Note: rect = rectangle; erd = exponential rise and decay; er = exponential rise; ed = exponential decay; Gau = Gaussian; prd = power law rise and decay; pr = power law rise; pd = power law decay

Table 2: Fitting parameters

Burst	C_0	t_1	t_0	σ	$\tau_{\theta,max}(\tau_{\theta,0})$	(χ^2, n)
GRB 910721	1930	1200	-0.658	0.197		(325.7, 701)
GRB 920925	27.6	204	-3.2		5.94	(342.5, 434)
GRB 930612	248	242	0	2.11		(785.4, 1308)
GRB 941026	2350	4110	-1.34		0.244(0.0732)	(945.2, 1983)
GRB 951019	1010	218	-0.489		0.518	(145.4, 258)
GRB 951102B	377	332	-0.653		0.824(0.418)	(70.39, 117)

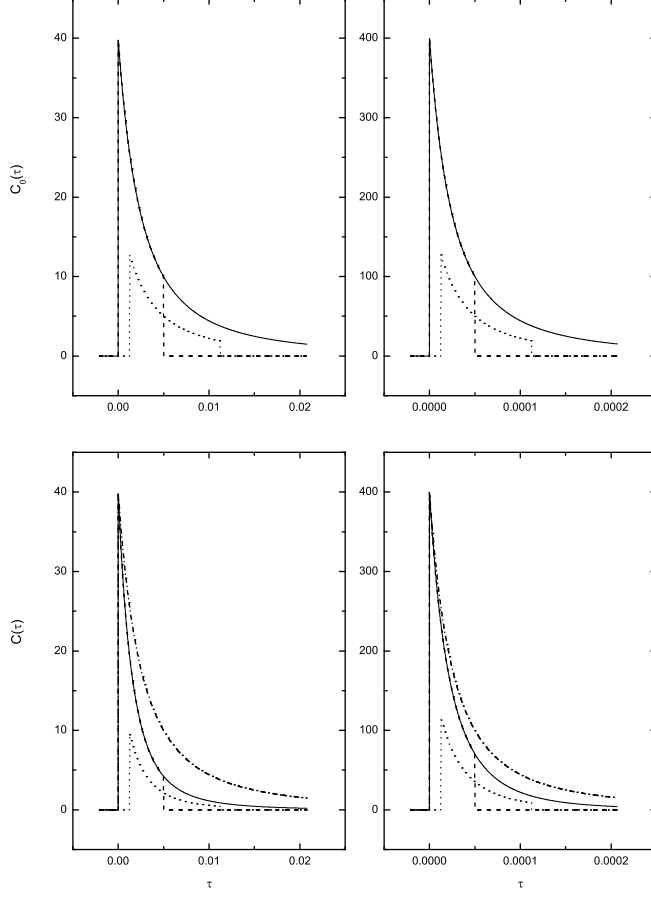


Figure 1: Plot of $C_0(\tau) - \tau$ for the light curve of the local δ function pulse determined by (36), with $\tau_{\theta,0} = 0$, $\Gamma = 10$ (upper left panel) and $\Gamma = 100$ (upper right panel), where the solid line represents the light curve arising from the radiation emitted from emitting area 1 [confined by (38)], the dash line stands for that from emitting area 2 [confined by (49)], and the dot line describes that from emitting area 3 [confined by (52)]; and plot of $C(\tau) - \tau$ for the light curve of the local δ function pulse determined by (35), where a Band function rest frame radiation form is adopted and we take $\tau_{\theta,0} = 0$, $\Gamma = 10$ (lower left panel) and $\Gamma = 100$ (lower right panel), where dash dot lines are the solid lines in the corresponding upper panels, the solid line represents the light curve arising from the radiation emitted from emitting area 1, which is normalized to the peak of the dash dot line, and the dash line stands for that from emitting area 2, and the dot line describes that from emitting area 3 (the dash line and the dot line shares the same magnitude constant of the solid line).

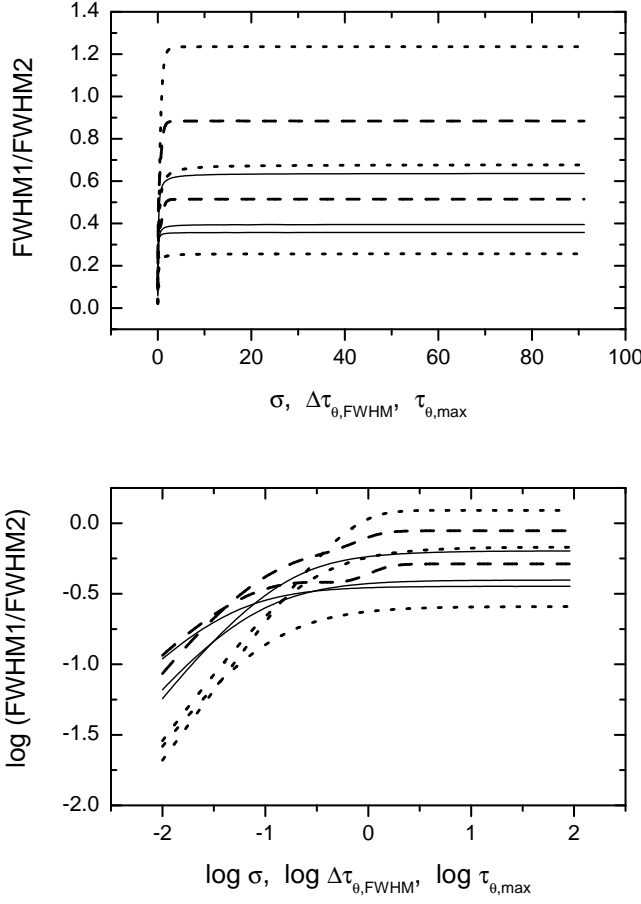


Figure 4: Ratio of the rising portion width to the decay phase width, $FWHM1/FWHM2$, of light curves vs. the local pulse width ($\tau_{\theta,max}$ for the rectangle local pulse, $\Delta\tau_{\theta,FWHM}$ for the three power law local pulses, and σ for other local pulses), for the eight forms of local pulses [where, solid lines from the bottom to the top represent local exponential rise and exponential decay pulse (81), local Gaussian pulse (84), and local power law rise and power law decay pulse (85), respectively; dash lines from the bottom to the top stand for local exponential decay pulse (83) and local power law decay pulse (87), respectively; dot lines from the bottom to the top denote local exponential rise pulse (82), local power law rise pulse (86), and local rectangle pulse (56), respectively] in both linear (the upper panel) and logarithm (the lower panel) formats.

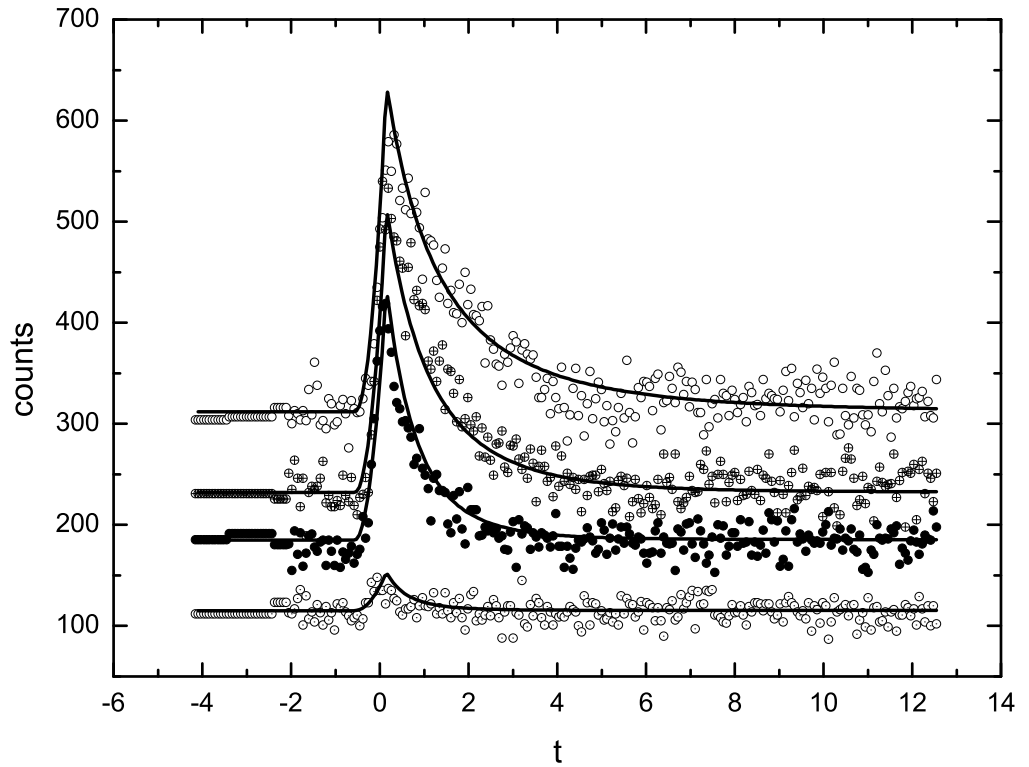


Figure 10: Fit to the four channel light curves of GRB 951019, where the fitting curves are calculated with the parameters of $\alpha_0 = -0.5$, $\beta_0 = -3.5$, $\Gamma = 100$, $\tau_{\theta, \min} = 0$, $\tau_{\theta, \max} = 0.518$, $\mu = 1$, $\nu_{0,p} = 0.907 \text{keV}$, $C_0 = 11.1$, $t_1 = 27600$ and $t_0 = -0.562$. The solid lines from the bottom to the top correspond to the fitting curves of channels 4, 3, 2 and 1, respectively. The circle and dot, filled circle, circle and plus, and open circle represent the count rates of the fourth, third, second and first channels, respectively.